



PERGAMON

Progress in Crystal Growth and Characterization  
of Materials (2002) 63–122

<http://www.elsevier.com/locate/pcrysgrow>

Progress in  
Crystal Growth  
and Characterization  
of Materials

# A REVIEW OF DEVELOPMENTS IN SHAPED CRYSTAL GROWTH OF SAPPHIRE BY THE STEPANOV AND RELATED TECHNIQUES

**Peter I. Antonov<sup>1</sup> and Vladimir N. Kurlov<sup>2</sup>**

<sup>1</sup> *A.F. Ioffe Physical-Technical Institute, Russian Academy of Science,  
St.-Petersburg, 194021, Russia*

<sup>2</sup> *Institute of Solid State Physics, Russian Academy of Science, Chernogolovka,  
Moscow distr., 142432, Russia. E-mail: kurlov@issp.ac.ru*

---

## Contents

1. Introduction	64
2. Variable Shaping Technique (VST)	68
3. Noncapillary Shaping (NCS)	70
3.1. Description of the technique	72
3.2 The growth of high quality shaped sapphire crystals with large cross-section.	76
3.2.1 The growth of crystals with a pre-determined cross-sectional shape	76
3.2.2 The growth of crystals with a variable cross-section	79
3.2.2.1 Growth near-net shaped dome crystals by the NCS technique	81
4. Growth from an Element of Shape (GES)	85
4.1 Control of gas bubbles	86
4.2 Growth near-net shaped dome crystals	90
4.3 Critical strain rate criterion for crack-free dome growth	93
5. Modulation-doped shaped crystal growth	95
5.1 Periodical doped structures	95
5.1.1 Obtaining periodic structures by the EFG technique	95
5.1.2 Obtaining layered crystals by the GES technique	97
5.2 Core-doped Fibers	100
5.2.1 Automatization as the base of high-quality core-doped fiber growth	102

5.3 Large composition-modulated shaped crystals	43
6. Shaped crystal growth with automated weight control	45
6.1 Process of automated crystal seeding	49
6.2 Crystal enlargement	50
6.3 Realization of automated control	51
7. Conclusions	56
Acknowledgements	56
References	56

## 1. Introduction

In 1938, Stepanov suggested, for the growth of shaped crystals and material structures, to form a melt column of a defined shape with the aid of a special shaper, and to subsequently crystallize the melt column outside the vessel walls. Liquid melt columns can be made of a variety of shapes by properly applying a high frequency electromagnetic field, by the use of the hydromagnetic effect, etc.

The development of the Stepanov method proceeded simultaneously along two lines: (1) development of technology for producing shaped single crystals, and (2) a study of the physical phenomena involved and development of a theory for the crystallization of shaped crystals. This included studies of the conditions of formation of the liquid melt column, the stability of the column, and the shape and properties of the grown single crystal.

In developing the technology for obtaining single crystals, most important is the correct choice of the version of Stepanov's method and of the shaper design. The structure of the material crystallized, the desired shape of the single crystal and interaction of the melt with the shaper play a predominant role.

Even in the first works by Stepanov and his coworkers the shaped crystals had been grown with the aid of nonwetted [1-4] and wetted [5] shapers. The crystal growth controlled by the melt-wetted shaper was studied both experimentally and theoretically.

The investigations devoted to the Stepanov method during this period one can find in numerous original papers.

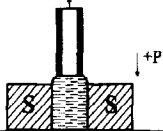
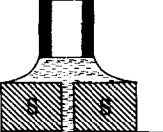
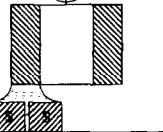
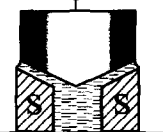
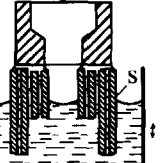
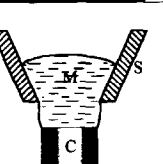
The materials of Conferences "All-Union Conf. On the Production of the Shaped Crystals and Products by the Stepanov Method and their Applications in the Nation Economy" were published in [6, 7].

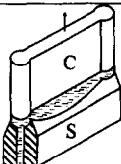
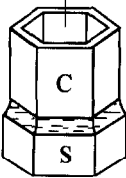
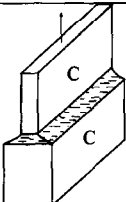

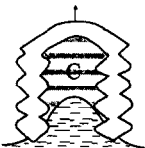
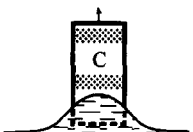
Special issue “Shaped Crystal Growth” was published in J. Crystal Growth [8] after appearance of numerous papers in this area. The first and the second International Symposiums on Shaped Crystal Growth (SSCG-1 and SSCG-2) were held in Budapest (Hungary) in 1986 and 1989. The proceedings were published in [9, 10]. Also several monographs [11–13] and reviews [14–17] about shaped crystal growth were published.

In our review we take your attention more distinctly to the papers which were not considered earlier. These works have a principal significance as well as for practical application and understanding the processes of crystallization from the melt.

Most useful versions of Stepanov Method are presented in Table 1.

Table 1. Various techniques based on Stepanov method.

1.	<b>S</b>	– Stepanov Classic Method		A.V. Stepanov, Soviet Phys.-JETP 29 (1959) 381. A.V. Stepanov, “The Future of Metal Working”, Leningrad, 1963, (in Russian).
2.	<b>EFG</b>	– Edge-defined Film-fed Growth		H.E. LaBelle Jr., A.I. Mlavsky, Nature 216 (1967) 574.
3.	<b>GES</b>	– Growth from an Element of Shape		P.I. Antonov, Yu.G. Nosov, S.P. Nikanorov, Bull. Acad. Sci. USSR, Phys. Ser., 49 (1985) 6.
4.	<b>NCS</b>	– Noncapillary Shaping Technique		V.N. Kurlov, Bull. Rus. Acad. Sci., Physics, 58 (1994) 1419.
5.	<b>VST</b>	– Variable Shaping Technique		D.Ya. Kravetskii, L.P. Egorov, L.M. Zatulovskii et al., Bull. Acad. Sci. USSR, Phys. Ser. 44 (1980) 126. V.A. Borodin, T.A. Steriopolo, V.A. Tatarchenko, Cryst. Res. Technol. 20 (1985) 833.
6.	<b>IS</b>	– Inverted Stepanov		K.M. Kim, S. Berkman, M.T. Duffy, A.E. Bell, H.E. Temple, G.W. Cullen, Silicon Sheet Growth by the Inverted Stepanov Technique, DOE/JPL-954465 (Final report, June 1977).

7.	<b>CAST</b> – Capillary Action Shaping Technique		<i>T.F. Ciszek, G.H. Schwuttker, J. Crystal Growth 42 (1977) 483.</i>
8.	<b>CS</b> – Closed Shaping		<i>L. Eriss, R.W. Stormont, T. Surov, A.S. Taylor, J. Crystal Growth 50 (1980) 200. D. Harkey, J. Crystal Growth 104 (1980) 88.</i>
9.	<b>RTR</b> – Ribbon-To-Ribbon float zoning		<i>I.A. Lesk, A. Baghadadi, R.W. Gurtler, R.J. Ellis, J.A. Wise, M.G. Coleman, in: 12<sup>th</sup> IEEE Photovoltaic Specialists Conf. Record, Baton Rouge, LA, 1976, p. 173.</i>
10.	<b>HRG</b> – Horizontal Ribbon Growth		<i>C.E. Bleil, J. Crystal Growth 5 (1969) 99. T. Koyanagi, in: 12<sup>th</sup> IEEE Photovoltaic Specialists Conf. Record, Baton Rouge, LA, 1976, p. 627.</i>
11.	<b>WEB</b> – Dendritic Web Growth		<i>S.N. Dermatis, J.W. Faust Jr., IEEE Trans. Commun. Electron. 82 (1963) 94. T.N. Tucker, G.H. Schwuttker, Appl. Phys. Letters 9 (1966) 219. D.L. Barrett, E.H. Myers, D.H. Hamilton, A.I. Bennett, J. Electrochem. Soc. 118 (1971) 952.</i>
12.	<b>ESP</b> – Edge Supported Pulling		<i>P.I. Antonov, Yu.G. Nosov, A.V. Stepanov, First Stepanov Conference, Leningrad, 1968, Ioffe Institute, p. 105 (in Russian). T.F. Ciszek, J.L. Hurd, in: Proc. Symp. Electronic and optical Properties of Polycrystalline or Impure Semiconductors and Novel Silicon Growth Methods, Eds. K.V. Ravi and B. O'Mara (Electrochemical Society, Pennington, NJ, 1980), p. 213.</i>

Stepanov Classic Method (1) was developed to produce a wide range of material structures from Al and its alloys. But this method for Al was unable to compete with industrial rolling methods except for specific shapes. At the same time the Stepanov Classic Method was useful for the economics single crystals of high value materials, in decreasing the waste of materials, and to make possible the production of complex shaped crystals even hard and fragile ones. Shaped single crystals of *Ge*, *InSb*, *GaAs* and others were grown by the Stepanov Classic Method. For *Si* ribbon 6–12 special versions were developed.

In 1967 LaBelle and Mlavsky reported on the growth of sapphire filament from the melt using a wetted die [18]. This method was called by Edge-defined Film-fed Growth (EFG), Table 1. EFG method initialized the development of other versions of shaped sapphire crystals which fulfilled the requirements for practical use.

Sapphire has a high refractive index and a broad transmission band spanning the ultraviolet, visible and infrared bands, a high hardness, melting point, very good thermal conductivity, tensile strength and thermal shock resistance. The favorable combination of excellent optical and mechanical properties of sapphire, complemented with high chemical durability make it an attractive structural material for high-technology applications. Sapphire crystals are used in medicine and blood chemistry as they are resistant to human blood and body fluids, and are totally impervious to moisture, and chemically inert. Frequently it is the combination of two, or more, of its properties that make sapphire the only material available to solve complex engineering design problems.

It is possible to note the next main directions in the field of the shaped crystal growth:

- 1) decrease the cost (increase of the productivity) due to the use of multiple crystal growth;
- 2) the growth of the crystals of complicated shapes;
- 3) growth of large-scale shaped crystals;
- 4) improvement of structure and quality of shaped crystals;
- 5) the growth of functional crystals(core-doped, layered crystals);
- 6) automatization of the crystal growth solves as well as shape control their quality, too.

So, the points 1-6 of the Table 1 will be considered in this review. Versions 3,4 and 5 will be described in more detail for shaped sapphire single crystals because in this area the problems of obtaining crystals of preset shape, control of single crystal structure perfection, defectiveness, optical and mechanical properties can be solved.

## **2. Variable shaping technique (VST)**

The development of modern science and technology requires the sapphire crystals of complex forms, namely, shaped crystals with variable cross-section.

The variable shaping technique (VST) enables one to vary the dimension and configuration of the crystal cross-section. This method allows one to obtain a gradual transition from one preset configuration of the crystal cross-section to another during one crystal growth process

It is well known that in the process of crystal growth by the EFG technique, the profile cross-section shape is mainly controlled by the die design, and its cross-sectional dimensions can vary only within very narrow limits restricted by the meniscus-existence zone, with the melt meniscus catching on the die free edge. Hence, the first attempt to widen the limits of varying pulled profile cross-sectional dimensions in the process of growth was to displace movable die elements [19]. Varying the cross-section was performed by using complex external and internal dies. The first one was used for tubular crystal growth. The second one was connected with a rod which could be shifted in an axial direction so as to move the top surface of these dies into and out of horizontal alignment with each other. When the internal die moved into alignment with external one the crystal grew as a circular rod.

Other techniques of varying the inner tube diameter are based on melt spreading from a circular capillary channel on the die top surface [20]. Initially, the melt film covers only part of the die top surface in the vicinity of the circular capillary channel and tubular crystal grow. Then the pulling velocity and the melt temperature are adjusted so that the surface tension will cause the film to spread toward the center of the die top surface. As a result, the cross-section of the crystal is changed. Both techniques allowed the translation from the tubular crystal to a circular rod in one process.

The next technique for discrete variation of the dimensions and geometry of the crystal cross-section during growth was based on the relative displacement of the elements of the thermal zone in a horizontal or vertical plane. This technique was proposed by Kravetskii et al. [21, 22]. Later the technique was developed by Borodin et al. [23–25].

In order to change the preset crystal shape during crystallization and to preserve the altered cross-sectional configuration during further growth, it is necessary to alter the geometry of the liquid meniscus. This technique consists of a sequence of steady state growth steps with different transition crystallization modes. During the transition the base of the meniscus moves across the top surface of the die assembly from one edge to the another, and the meniscus mass is altered. One of the schemes of VST with a changeable crucible position is illustrated in Fig. 1 [25].

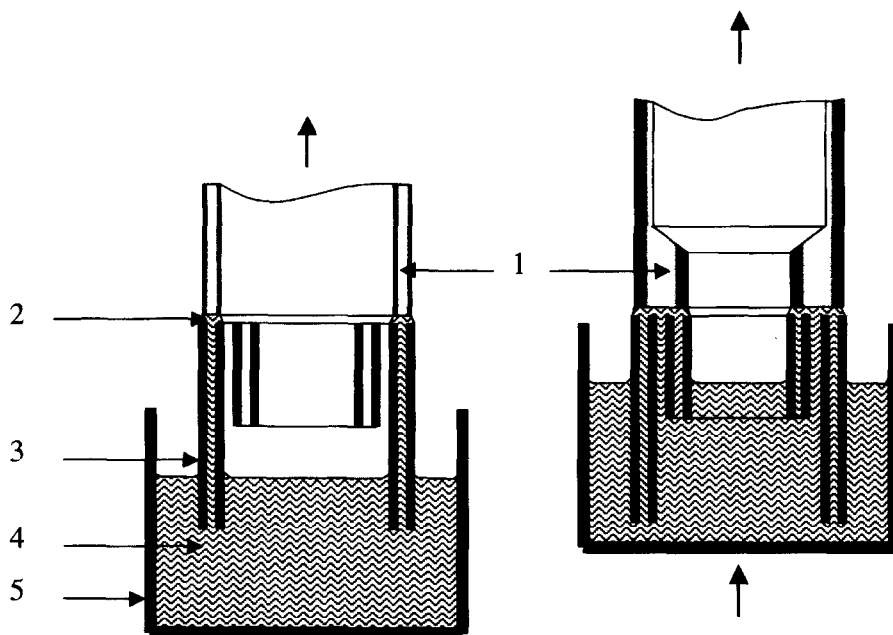


Fig. 1. The scheme for the variable shaping technique using displacement of the crucible:

1 – crystal, 2 – meniscus, 3 – die, 4 – melt, 5 – crucible.

The sequence of operations to alter the crystal cross-sectional configuration is shown from the left to right. The set of dies is not connected with the crucible. So, the crucible can be translated along the vertical axis relative to a fixed position of the die assembly. The dies should be of different lengths so as to provide separate dipping of their lower parts into the melt. To realize the shape transition mode the lateral surfaces of the neighboring dies are separated by narrow gaps which can serve as capillary feeding channels for the melt. When the crucible is raised so that the next die is dipped into the melt, the capillary gap supplies an additional mass of melt to the top of the die assembly. This portion of the melt contacts the already existing meniscus and with the edge of the die just dipped into the melt. As a result, a new type of meniscus forms, and the growing crystal alters its shape which is controlled by the dies dipped into the liquid. If the crucible is lowered, so that one of the dies is withdrawn out of the melt, the pulled crystal will suck the rest of the melt out of the die capillary channel and out of the capillary gap between the neighboring dies. In this case the base of the meniscus will move to the top surface edges of the die which is still dipped in the melt. This causes the alteration and reduction of the crystal cross-section

Sapphire shaped crystals grown by the variable shaping technique are shown in Fig. 2. Sapphire crucibles, boats, caps for thermocouples, crystals with the change-over from rectangular cross-section to tube, tubes with a predetermined alteration inside and outside diameters, tubes with attachment of side ribs, envelopes for high-pressure sodium lamps were grown by VST.

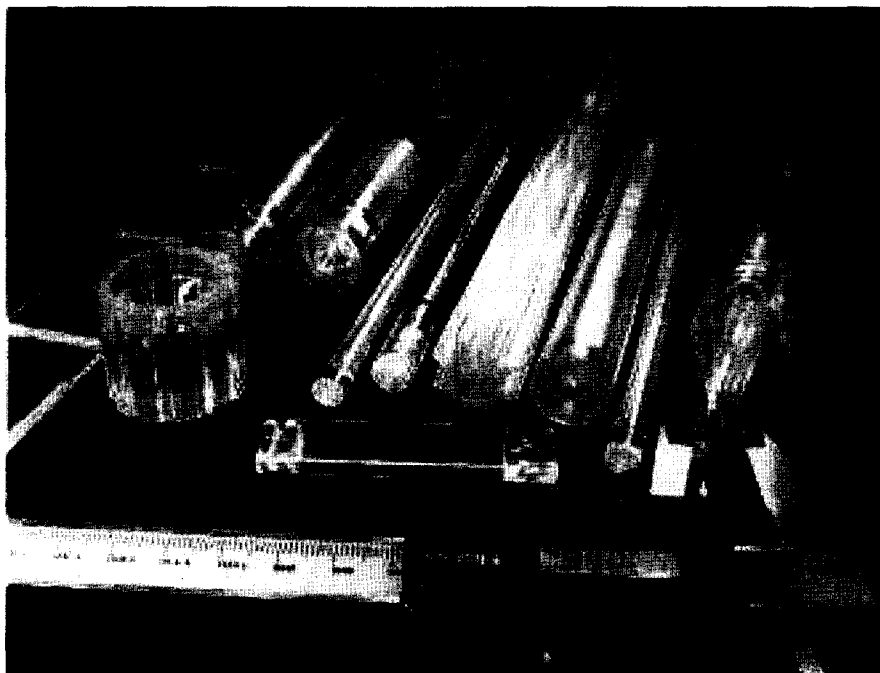


Fig. 2. Sapphire shaped crystals grown by the VST.

### 3. Noncapillary shaping (NCS)

One of the basic defects in crystals grown from a melt, are gas bubbles, which appear at some critical supersaturation of the melt with a gas impurity whose distribution coefficient is usually less than unity. In this case the homogeneous nucleation and growth of a gas bubble can take place in the impurity-enriched zone ahead of the crystallization front [26, 27]. Distribution of the gas-forming impurity ahead of the crystallization front in Czochralski growth depends on the character of the



forced melt convection. This character is mainly defined by the crystal rotation [28]. Melt stirring in the proximity to the crystallization front sweeps away the impurity-enriched zone decreases the amount of impurities at the crystallization front. Therefore, melt stirring decreases the probability of the gas-forming impurities in a crystal.

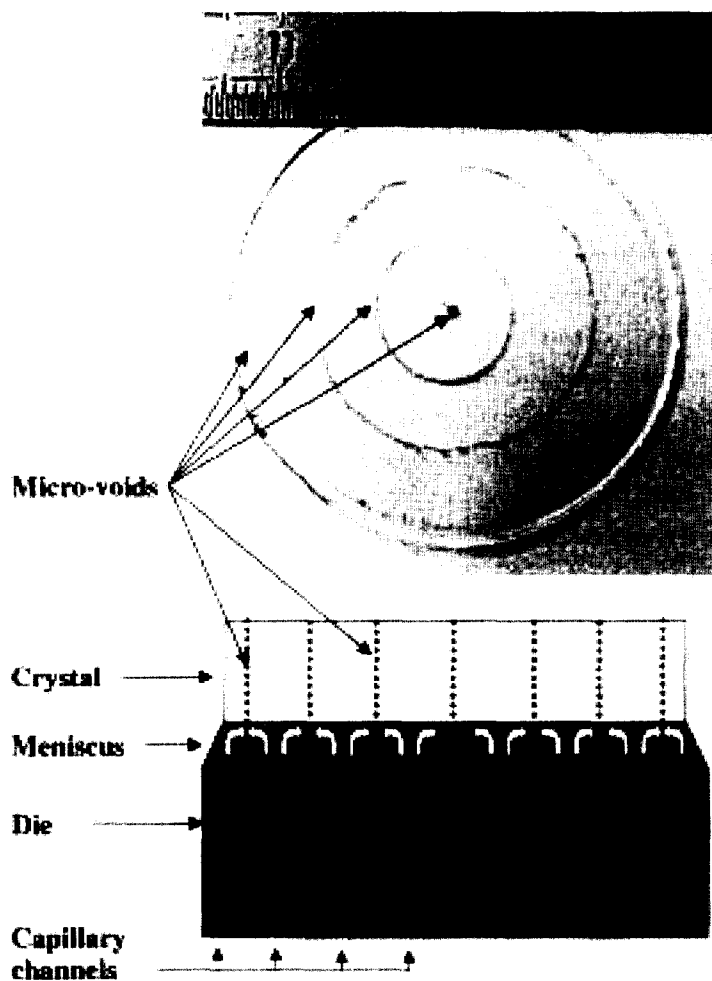


Fig. 3. Distribution of gas bubbles in the cross-section of a sapphire rod of 40 mm diameter, grown using a die with 4 ring-shaped capillary channels.

The growth of shaped crystals by the EFG method with a die wetted by melt and with a capillary feeding system does not allow impurities to be removed from the crystallization front. In this case the distribution of gas bubbles is determined by hydrodynamic flows of the melt in the neighbourhood of the crystallization front and thus a die's design plays an important role. The dependence of the gas bubbles and dopant distribution on the geometry of the capillary channels in the dies has been observed earlier when growing shaped silicon and sapphire crystals [29–34].

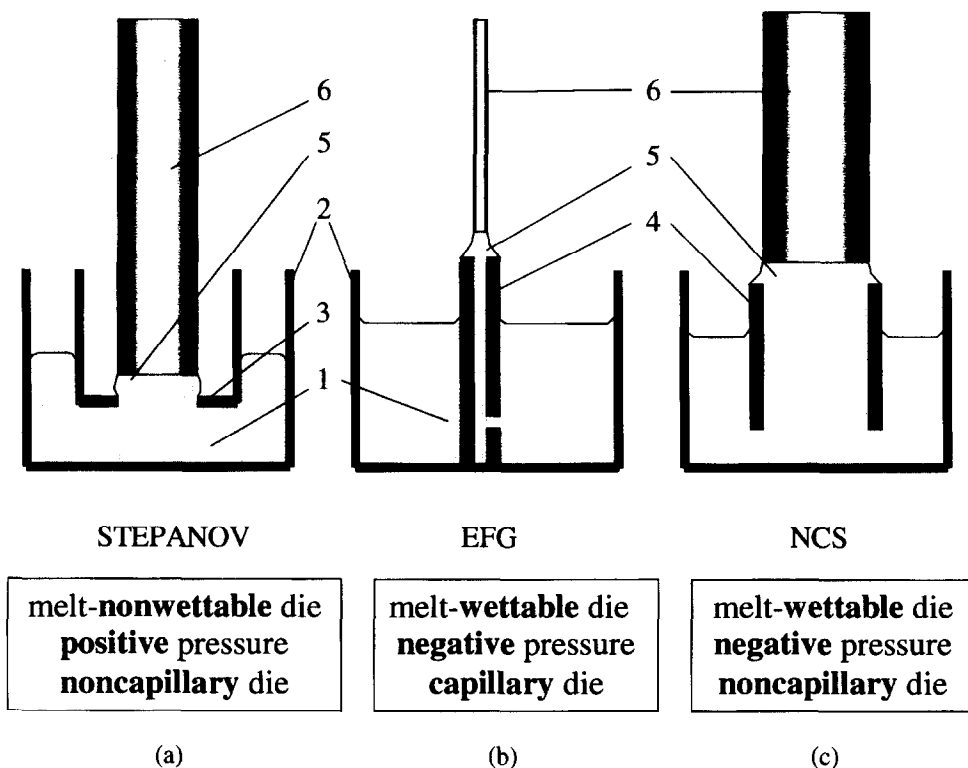
Fig. 3 shows the cross-section of a sapphire rod 40 mm in diameter grown from a die with four-ring capillary channels. The superposition of a sapphire disk onto the top surface of the die shows that the pile-up of gas bubbles in the disk are located at the sections where melt flows moving from the capillary channels meet each other. An analogous situation has been observed when growing sapphire rods of 12 mm diameter from a die with a ring capillary channel or from one made from cuts of a molybdenum wire placed in a cylindrical band [31]. The authors [31, 32] showed analytically that the regions with an enhanced concentration of gas impurities driven back by the interface surface are adjacent to those regions of the crystallization front under which the components of the velocity of the melt flow are minimum. Areas with minimum velocity of radial flow are formed by intersecting melt flows which spread over the top surface of the die. These areas are sites of most probable generation and capture of gas inclusions.

The character of interaction of melt flows at their meeting place can be explained by analogy to an interfacial phenomenon. The velocities of the melt flows from capillaries differ in size and direction. Due to the viscosity of the melt the flows will slow down each other at their meeting place. The vectors of the velocities have different directions and form pairs of forces rotating layers of flow that result in the formation of vortices, Fig. 3.

So, one of the main problems of high quality shaped crystal growth is how to prevent the formation of gas bubbles and other inclusions, which are formed in these regions having minimum components of melt velocity ahead of the crystallization front.

### ***3.1. Description of the technique***

The primary difference [30] between LaBelle's EFG process and Stepanov's early work is the follows: the EFG process must use a wettable die and the Stepanov technique generally used a non-wetted shaper. For melt-nonwetable materials, the melt column should be embraced from outside providing additional pressure on the liquid to make the melt-shaper contact point touch the shaper sharp edge [35], Fig. 4a. For melt-wettable materials, the melt column has negative pressure using the capillary die, Fig. 4b.



4. The schemes of Stepanov (a), EFG (b) and NCS (c) methods: 1 – melt; 2 – crucible; 3 – non-wetted shaper; 4 – wettable die; 5 – meniscus; 6 – crystal.

As distinguished from the technique based on the traditional capillary feed, the NCS method ensures the absence of micro-voids, gaseous and solid inclusions, which are formed in the regions with minimum components of melt velocity ahead of the crystallization front. The dominant flow always moves from the center to periphery irrespective of crystal cross section, thus enabling the growth of large sapphire crystals free of bulk inhomogeneities. The forming of the optimal interface surface and the hydrodynamic flows of melt ahead of the crystallization front are determined by shape of the top surface of the die, by the velocity of growth, and by the size of noncapillary channel.

The NCS method was developed for the growth of high quality shaped sapphire crystals with large cross-section. This method uses a wettable die. However, in contrast to the EFG method the NCS technique does not use the lifting of the melt from the crucible to the die-top through a capillary

channel. But at the same time the melt column has a *negative* pressure as for the EFG method. The main feature of this technique consists in the delivery of the melt to the growth interface through a *noncapillary* channel via a *wettable* die, Fig. 4c. The word "noncapillary" means here that the diameter of channel is greater than a value of the capillary constant.

But how can one make possible the lifting the melt to the crystallization front through a noncapillary channel via a wettable die?

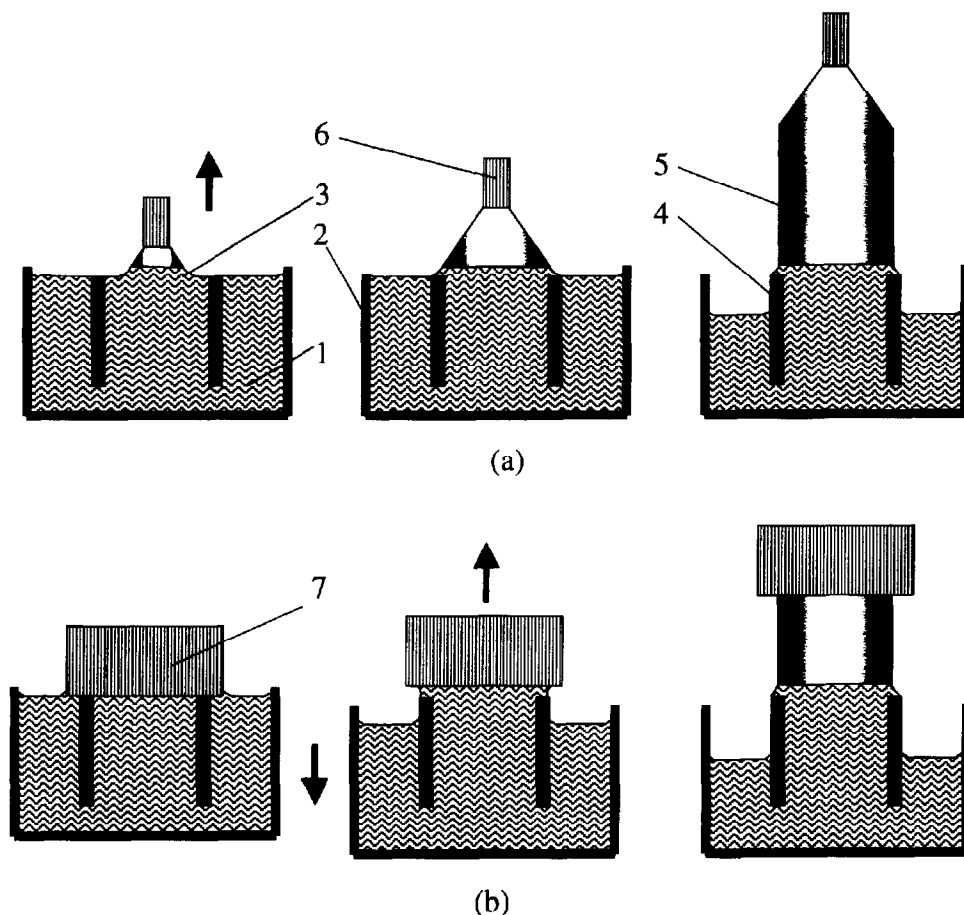


Fig. 5. The sequence of bulk crystal growth stages by NCS method using different seed shapes: with the use of a point seed (a); with the use of a bulk seed (b). 1 – melt; 2 – crucible; 3 – meniscus; 4 – die; 5 – crystal; 6 – point seed; 7 – bulk seed.

Fig. 5 shows the sequence of bulk crystal growth stages by the NCS method using different seed shapes. At the beginning of the process the die top is level with the melt in the crucible. By using a point seed (Fig. 5a), a crystal enlarges up to the edges of the die during an initial stage. After that the melt level in the crucible can be lowered relative to level of the die top. The melt rises to the crystallization front through the central noncapillary channel. Initially this version was used for growth of  $\text{CaF}_2$  crystals 20 mm in diameter [36].

Also a wettable rod can be used as a seed (Fig. 5b). The melt level in the crucible can be lowered after the seeding process.

The particular case of the seeding using both capillary and noncapillary channels is described in Ref. [34]. The lifting of the melt to the crystallization front inside a noncapillary channel is achieved by the pressure difference between the growth chamber and the inside the closed volume under the seeding plate. The melt arriving through the noncapillary section of the die joins the melt meniscus coming through the ring capillary channel, which results in the growth of crystal in the shape of a monolithic rod, Fig. 6. To create the closed volume, the seeding is performed over the entire perimeter of a ring capillary channel, Fig. 6a. In the initial stage, when the melt approaches the crystallization front only through the capillary feed, a hollow crystal grows. The closed volume below the seed begins to increase and the pressure decreases according to the Boyle-Mariotte law. The resulting difference in pressures forces the melt to lift inside the noncapillary section of the die, Fig. 6b. Upon further pulling, the melt arriving through the noncapillary section of the die joins the melt meniscus coming through the ring capillary channel, which results in the growth of a crystal in the shape of a monolithic rod, Fig. 6c.

The distance  $l$  between the seeding point and the beginning of the monolithic rod depends substantially on the pressure  $P$  in the growth chamber. The distance  $l$ , assuming that the crystallization of the melt arriving from both capillary and noncapillary sections occurs at the same level from the die top,

$$l = \frac{H}{1 - (H_f \rho g / P)} - H + H_f,$$

where  $H$  is the distance between the level of melt in crucible and the top of the die,  $H_f$  the distance between the melt level in crucible and the crystallization front,  $\rho$  the melt density,  $g$  the gravitational constant.

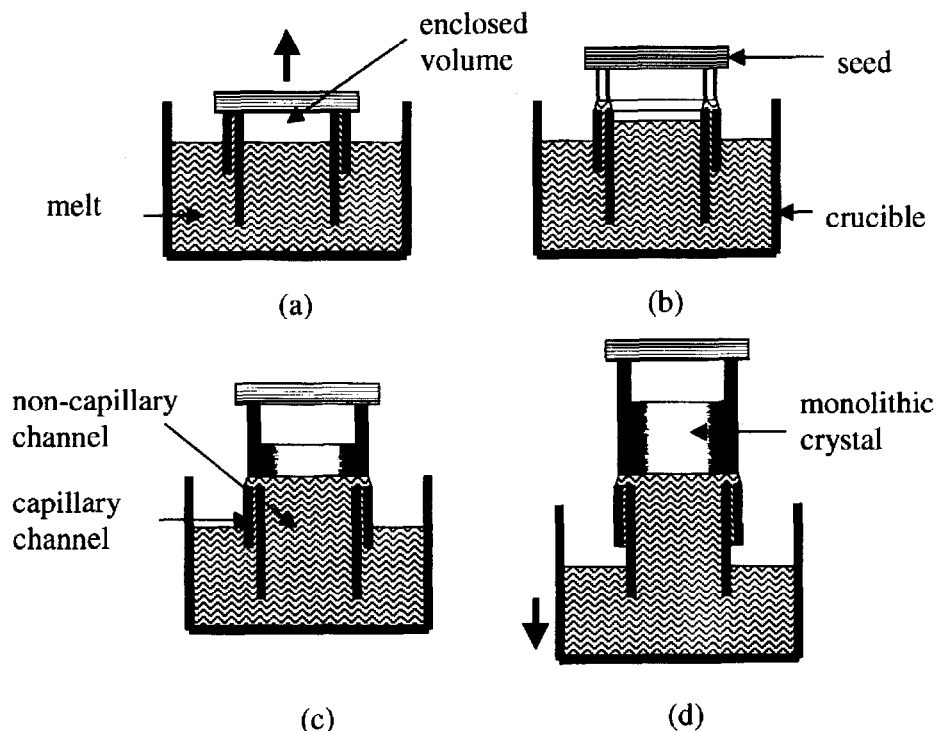


Fig. 6. The scheme of monolithic crystal growth by the NCS method using the pressure difference in a growth chamber and inside a closed volume under a seeding plate: (a) seeding, (b) growing a hollow closed shape, (c, d) growing a monolithic crystal.

### 3.2 The growth of high quality shaped sapphire crystals with large cross-section

#### 3.2.1 The growth of crystals with a pre-determined cross-section shape

The formation of the optimum interface surface and the hydrodynamic flows of melt in the neighbourhood of the crystallization front are determined by the shape of the top surface of the die, and by the relationship between the crystal cross-section, velocity of growth and size of the central oncapillary channel.

When the monolithic rod starts growing, the crystallization front is fed with melt through the ring capillary and central noncapillary channels, Fig. 6b. The regions in which these flows join are characterized by a minimum in the resulting velocity. In these areas homogeneous nucleation, growth and capture of gas bubbles by the crystallization front is likely to occur (Fig. 3). Fig. 7 (at the left) shows the characteristic ring-shaped porous regions in the cross-section of monolithic sapphire crystals grown under simultaneous melt feeding from the capillary and noncapillary channels of dies with different geometries. The distribution of gas bubbles (width of a ring, its location, etc.) depends on the position of capillary channel and the velocity components of melt flows below the crystallization front.

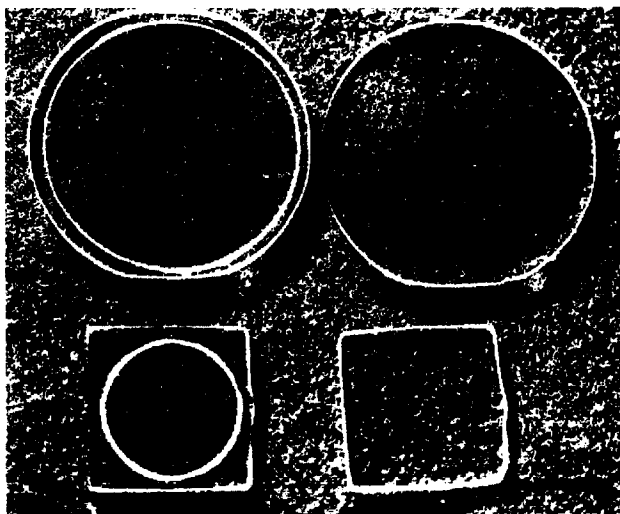


Fig. 7. Cross-sections of sapphire crystals grown by the NCS method: crystals grown with simultaneous feed from capillary and noncapillary channels (at the left) and using feed provided only from a noncapillary channel (at the right).

However, the most important aspect of this method is that it allows the production of crystals completely free of gas bubbles whose origin is connected with the presence of regions characterized by a minimum in the melt flow velocities. This is achieved either by the suppression of capillary flow from the noncapillary channel, or by shutting off the capillary feed; then the crystal grows only from the melt fed from the noncapillary channel, Fig. 6d. The melt moves only from the center to the

periphery, in this case the free surface of the meniscus is the sink for gaseous impurity, which results in the absence of bubbles both in the center of the monolithic crystal, and next to its surface, Fig. 7 (at the right).

Cylindrical rods up to 40 mm in diameter for optics and rods of other shapes which may be used in optics and jewellery were grown by the NCS method, Fig. 8. The investigation of the grain structure of the sapphire crystals grown by the NCS method has shown a misorientation of less than  $1^\circ$  between the grain boundaries over a finite length of the grown rods (150–300 mm).

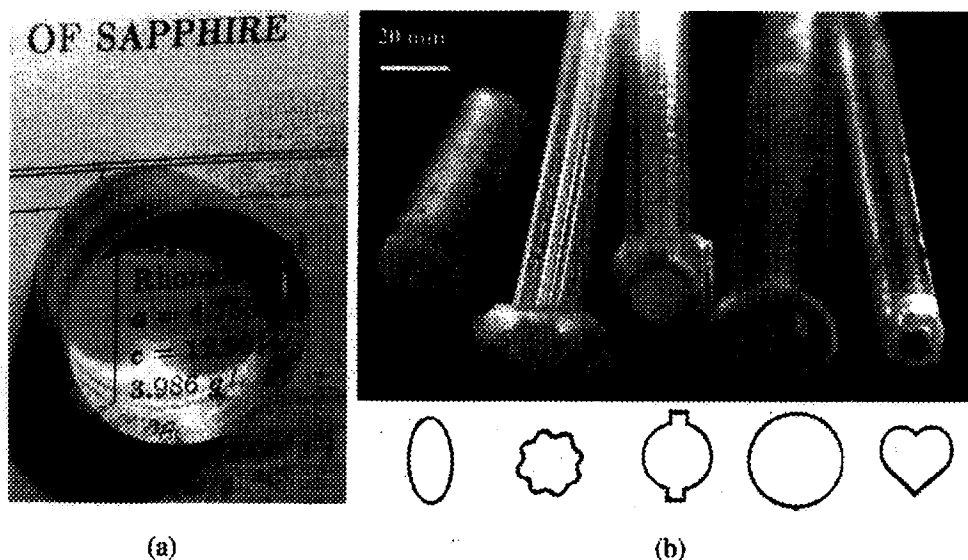


Fig. 8. Shaped sapphire single crystals grown by the NCS method: (a) sapphire bulk crystal of 35 mm diameter using feed provided only from a noncapillary channel; (b) rods of various shapes (at the bottom, cross-sections of the grown profiles are shown).

The method based on noncapillary feed is applicable to the growth of thick walled tubes (Fig. 9) and plates without gas bubbles in their volume. The noncapillary channel is arranged between the two capillary ones, or some others of more complicated profiles, which we may "switch off" or "switch on" again as capillary or noncapillary channels.



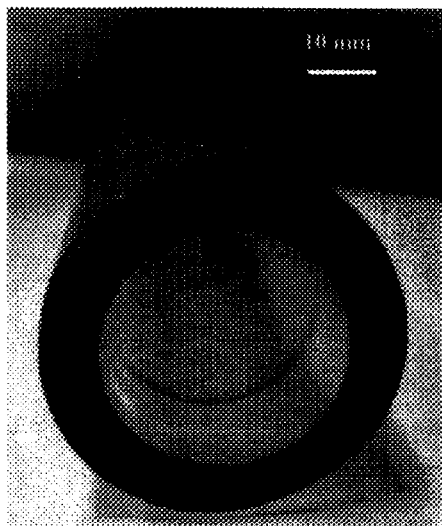


Fig. 9. Thick walled sapphire tube grown by the NCS technique.

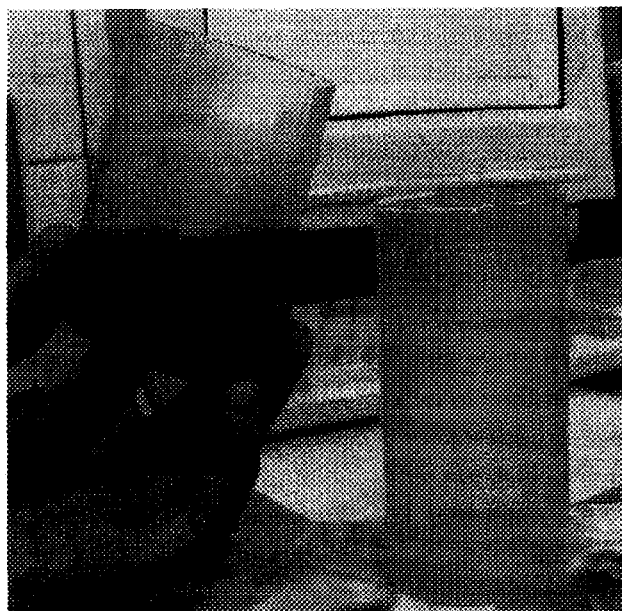
### *3.2.2 The growth of crystals with a variable cross-section*

Also the NCS technique allows change from one shape to another. We can achieve growth from a solid crystal to a hollow one (the feed of melt proceeds only from the ring capillary) and vice versa [33, 34]. Sapphire crucibles were grown early using capillary and noncapillary replenishment [37]. The NCS method produces a wide range of sapphire crystals similar to the variable shaping technique [21, 24] and it has vastly increased the dimensions of grown crystals. The essential difference between the crystals grown by the NCS method and those produced by the variable shaping technique is the absence of gas bubbles in the crystal volume.

Fig. 10 shows sapphire crucibles grown by the variable shaping technique (on the left) and those - by the NCS method (on the right). The arrow indicates a typical column of gas bubbles in the bottom part of the crucible grown by the VST method. Bubbles of this type are absent in the bottom section part of the sapphire crucible grown by the NCS method. Consequently, this method is good for growing sapphire crucibles with transparent (free of gas bubbles) bottoms and crystals of variable cross-section of other shapes without gas bubbles in their volume. Fig. 11 shows sapphire crucibles 65 mm in diameter.



Fig. 10. Sapphire crucibles grown by: the variable shaping technique, external diameter is 13 mm, the arrow indicates a column of gas bubbles (at the left); and those grown by the NCS method, external diameter of the crucible is 34 mm (at the right).



The NCS method was used to grow sapphire rods and tubes with internal and external threads, Fig. 12. This method allows a change in the pitch of thread (at the bottom of figure) during the growth process.

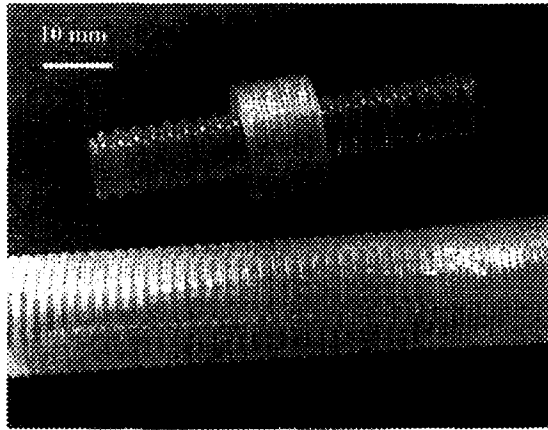


Fig. 12. Sapphire crystals with internal and external threads grown by the NCS method.

### 3.2.2.1 Growth near-net shaped dome crystals by the NCS technique

Besides the controlled lateral form of the crystal, one can obtain controlled formation of the joint between the hollow part of a crystal and a solid region and vice versa. Combinations of this control with the possibility to produce the crystals without gas inclusions in their volume by the NCS method enables the growth of near-net-shaped domes [38].

The main design feature of the die was a hemispherical top for the inner thick-wall liner with a noncapillary channel (Fig. 13). The die was also provided with the capillary channel along its perimeter. The height of the hollow spherical segment  $h$  was

$$h = \sqrt{d(2R - d)},$$

where  $R$  is the radius of the spherical segment,  $d$  - required thickness of the blank wall.

At the initial stage, after the formation of a ring meniscus between the seed plate and the die (Fig. 13a), the melt approaches the crystallization front only through the capillary feed, and the crystal grows in a tube-shape (Fig. 13b). As the enclosed volume increased, the difference between the gas pressure in the enclosed volume and that in the growth chamber also grew. Due to this pressure difference, the melt rose in the hole and then in the liner cavity.

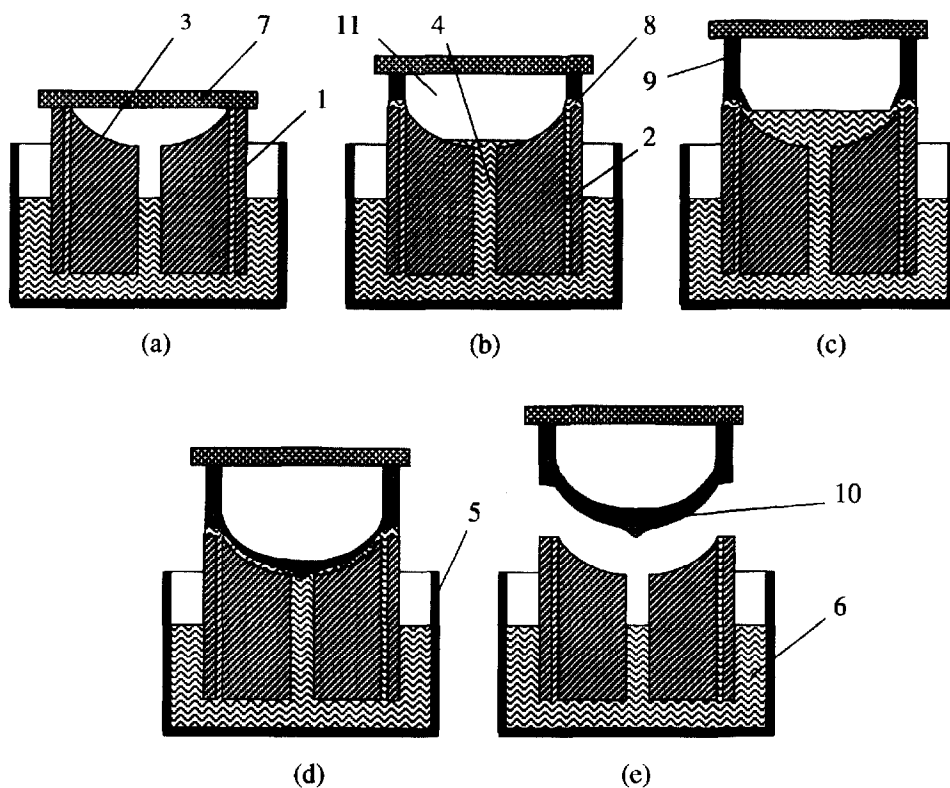


Fig. 13. The sequence of individual near-net-shaped dome growth stages. 1 – die; 2 – ring capillary channel; 3 – liner cavity; 4 – noncapillary channel; 5 – crucible; 6 – melt; 7 – seed-plate; 8 – ring meniscus; 9 – tube-shaped crystal; 10 – near-net-shaped dome; 11 – enclosed volume.

When the melt in the cavity reached the edges and met with the meniscus, the hemispherical part of the blank (Fig. 13c) began crystallizing. The shape of the inner surface of the blank depended on the rate of pulling and radial temperature gradient. Under proper thermal conditions this shape may resemble that of the crystallization front. The front surface reflects the hemispherical configuration of the liner top (Fig. 13d). As soon as the stage *c* began, we pulled the crystal to a length equal to the height  $h$  of the spherical segment. Then we abruptly broke the hemispherical sapphire blank from the die top (Fig. 13e).

Fig. 14 shows the as-grown near-net-shaped hemispherical sapphire blank with the seed plate. Fig. 15 shows the cross section of a near-net-shaped dome grown by the NCS method. The surface sections to be removed mechanically for fabricating a final-shaped dome are shaded. This shows that the surfaces can be controlled accurately so that minimum grinding and polishing will be necessary to produce the finished domes. Final-shaped sapphire domes fabricated from near-net-shaped blanks and) conoscopic figure from the sapphire dome are shown in Fig. 16. High-quality near-net-shaped sapphire domes up to 80 mm in diameter were grown by the NCS method.

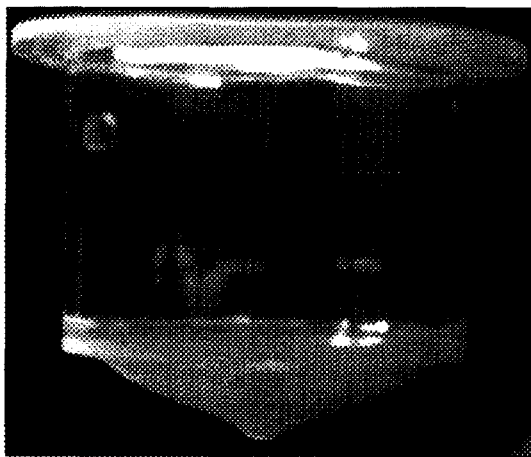


Fig. 14. The as-grown near-net-shaped sapphire dome grown by the NCS method.

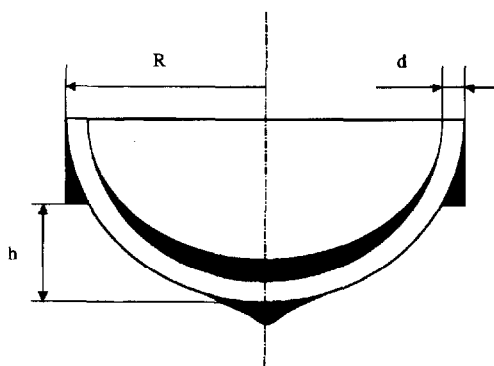
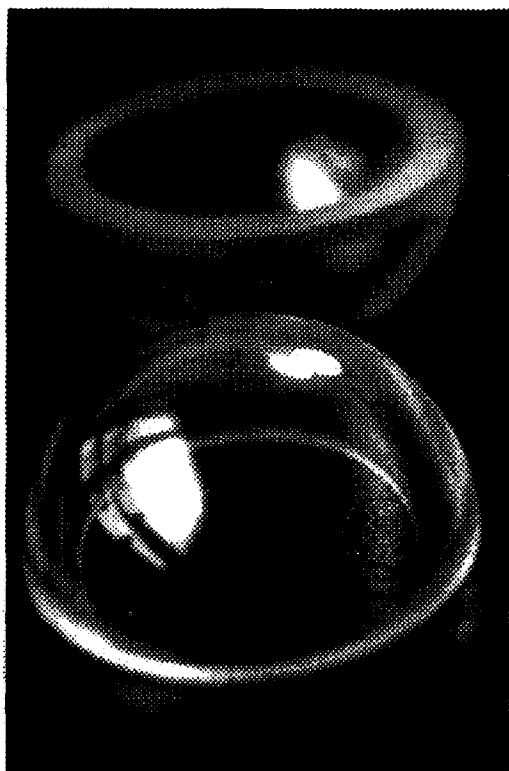
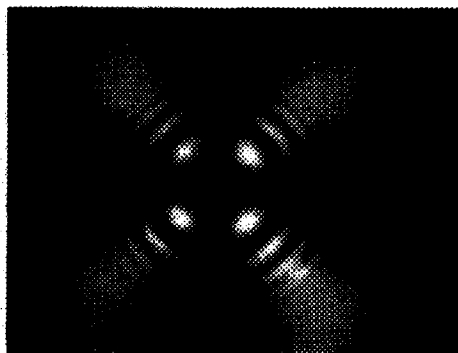


Fig. 15. Scheme of a near-net-shaped dome cross-section grown by the NCS method.



(a)



(b)

Fig. 16. (a) Mechanically finished hemispheres produced by the NCS method. (b) Conoscopic figure from sapphire dome grown along c-axis (photograph taken with dome between crossed polarisers).

Experiments were also carried out to obtain a set of near-net-shaped domes during one growth cycle for additional cost saving in crystal growth. The NCS method allows the passage from a solid crystal to a hollow one (the feed of the melt proceeds only from the ring capillary) and vice versa [38]

#### 4. Growth from an Element of Shape (GES)

Stepanov was the pioneer of the shaped crystal growth field [3]. He formulated a crystal-shaping principle, namely that the *shape or an element of shape* to be produced is created in the liquid state by means of various effects enabling the liquid to retain that shape, and then the shape or element is converted to the solid state by the use of appropriate crystallization conditions. This principle indicates that two modes of capillary shaping can be used in pulling a crystal from the liquid on a seed: producing a meniscus whose shape completely coincides with that of the grown crystal and producing a meniscus representing a small element in the crystal shape.

The Growth from an Element of Shape (GES) method has been developed on the base of Stepanov method and its main principles were described by Antonov et al. [39]. It consists of pulling a shaped crystal from a melt meniscus, which is only a small element of the whole transverse cross-section configuration of the growing crystal. The crystal grows layer-by-layer and the period  $l$  is determined by the ratio  $V/\omega$ , where  $V$  is the pulling rate and  $\omega$  is the rotation frequency.

The first experiments were made to grow lithium fluoride single tubular crystals [39]. Between the surface of the seed and the shaper there is a column of liquid, which is a small element of tubular form for the future crystal, Fig. 17. When the seed is rotated, its horizontal surface contacts the meniscus in the column, and a thin layer of liquid is formed.

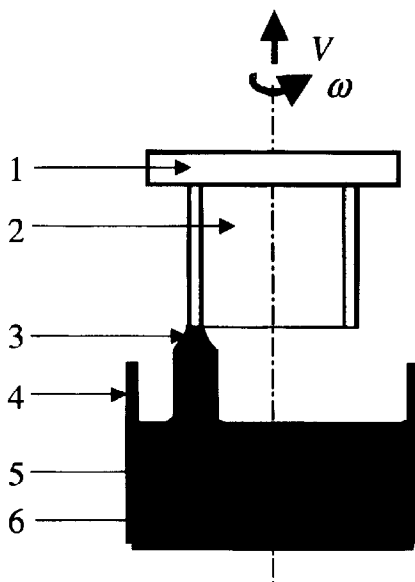


Fig. 17. The scheme for the GES method. 1 – seed plate, 2 – tubular crystal, 3 – meniscus, 4 – crucible, 5 – die, 6 – melt.

But the major development of the GES method was achieved for growing complicated sapphire crystals with continuous alteration of the lateral surface profile. Sapphire is the most durable and commercially available middle infrared (IR) window material. One of the most important applications are domes for relatively high-speed missiles and the main problem is to obtain transparent materials that have good high-temperature properties and good resistance to rain and other sources of damage. A new approach to produce sapphire at reduced cost is to grow a near-net-shaped crystal. Methods for the preparation of near-net shapes directly in the course of the growth process by HEM (heat exchange method) [40], GSM (gradient solidification method) [41], NCS (noncapillary shaping) [38] and the modified EFG (edge-defined film-fed growth) method [42] have been reported in the course of the last few years. Nevertheless, so far the development of a process for low cost sapphire near-net-shaped domes remains an unsolved problem.

Authors of the GES method report that small liquid volumes can be continuously solidified after combined displacements of the seed relative to the die, in order to produce crystals with complicated shapes. During the growth, the displacement may be applied to the seed or the die, or to both simultaneously [43].

Sapphire tubes and other hollow revolving bodies were first grown by Borodin et al. [44]. They used the term *local shaping technique (LST)* instead of the GES term.

To alter the profile of a lateral surface according to a preset program they used horizontal die displacement relative to the crystal rotation axis, [25]. Following variation of the horizontal die coordinate the inner and the outer radii of the sapphire tube being pulled alter, and the profile of the lateral surface changes accordingly.

The alternative is to use horizontal displacement of the seed during the growth process. A special apparatus design with horizontal translation of the pulling shaft, added to the usual vertical and rotating movements, was applied for producing sapphire crystals of complicated shape [45].

However, for the preparation of high-quality sapphire hemispheres applicable to high-temperature optics it was necessary to solve the following tasks: 1) growth of GES crystals free of gas bubbles and solid inclusions in their volume; 2) growth of near-net-shaped blanks close to dome shape; 3) growth of crack-free sapphire hemispheres.

#### **4.1 Control of gas bubbles**

GES crystals grew layer by layer with each of them having a thickness determined by the pulling and rotation rates ratio:  $V/\omega$ . As a consequence, GES sapphire crystals contained regular striations and a band-like distribution of voids described in reference [44] as gas bubbles, solid



inclusions and inhomogeneous doping impurities. On the one hand, argon, nitrogen, carbon oxides, molybdenum oxides and products of the alumina dissociation may contribute to striation forming. On the other hand, the striations may be caused by structural imperfections as well; a configuration of the void pile-ups is often followed by that of striations.

The regular striations and band-like distribution of voids observed in the longitudinal sections of the sapphire tubes (Fig. 18) display a spiral distribution of these defects in the bulk of the crystal, with the angle of the spiral line slope given by  $\alpha = \tan^{-1}(V/2\pi R\omega)$ , where  $R$  is the distance from the rotation axis of the seed holder to the axis of the die.

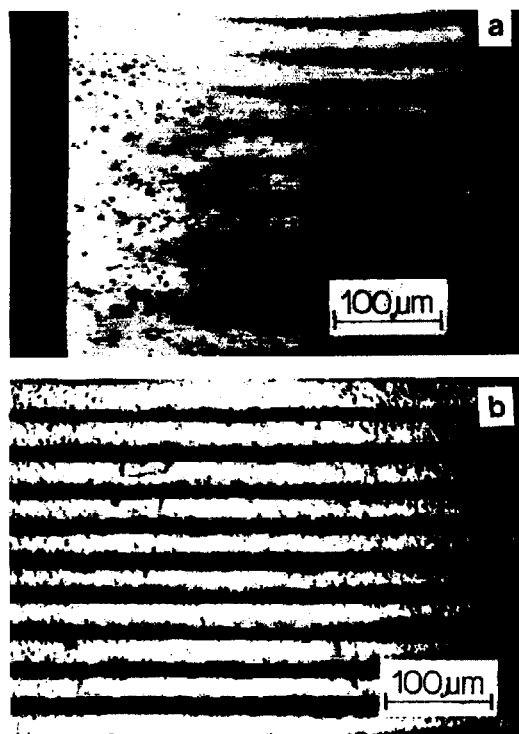
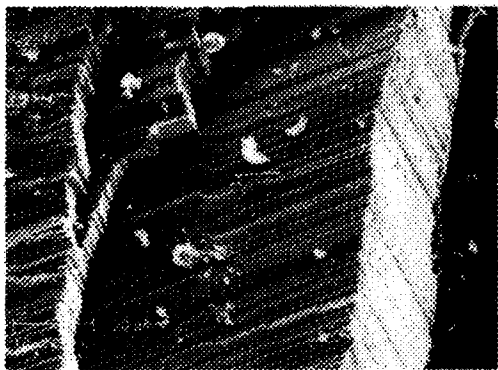
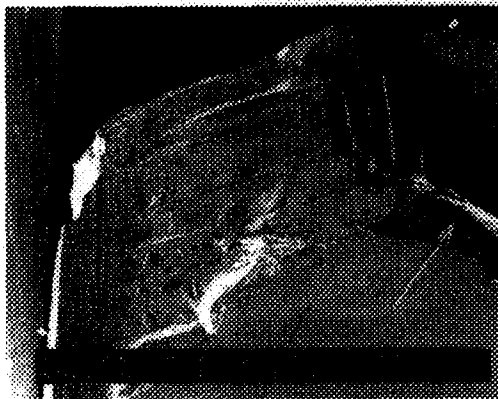


Fig. 18. Longitudinal sections of a sapphire tube: (a) regular pile-ups of voids and surface relief seen in the wall thickness; (b) lateral surface relief on the tube surface [44].



(a)



(b)



(c)

The arrangement and dimension of voids in the crystal are determined by the morphology of the solid-liquid interface, the period  $V/\omega$ , and the linear growth rate  $V_\omega = 2\pi R\omega$ . These defects sharply decrease the optical and mechanical properties [46] of the material. In GES crystals the stairs were observed on the fracture surface (Fig. 19a). The height of the stair is correlated with the height of the layer. Therefore the crack propagates in some jumps from one level to another. An origin of failure is a zone of high concentration of voids (Fig. 19c). The location of the zones coincides with the bubbles distributed along each new crystallized layer. Partial removal of stress is observed in GES crystals before destructive failure, Fig. 20. It occurs as a result of the interaction of a crack with defective layers (proof by observation of a fracture surface – see Fig. 19) that results in the partial loss of energy of the crack.

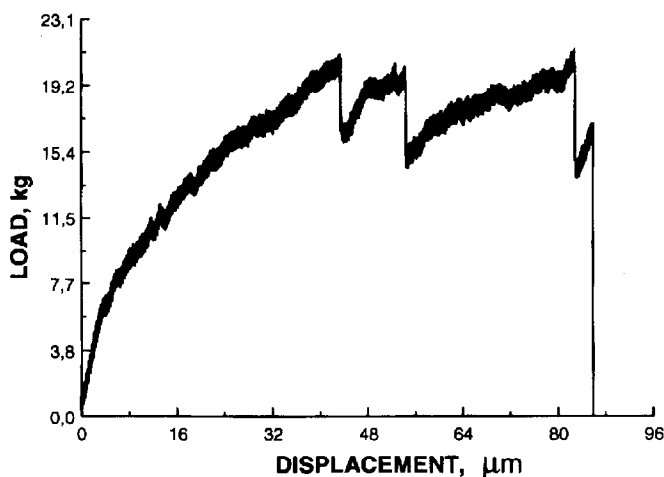


Fig. 20. Fracture curve of a GES crystal.

So, it is very important to find the optimum regimes that lead to GES sapphire growth without striations.

It was found that a marked decrease in the linear growth rate and period  $V/\omega$  leads to improved GES crystal quality. Fig. 21 shows a longitudinal cross-sections of a sapphire GES crystal which was grown using a low frequency of rotation (1 rpm) rate [45]. The ratio  $V/\omega$  was reduced (Fig. 21a to Fig. 21b) down to  $4 \mu\text{m}$ , to obtain GES crystals completely free of voids.

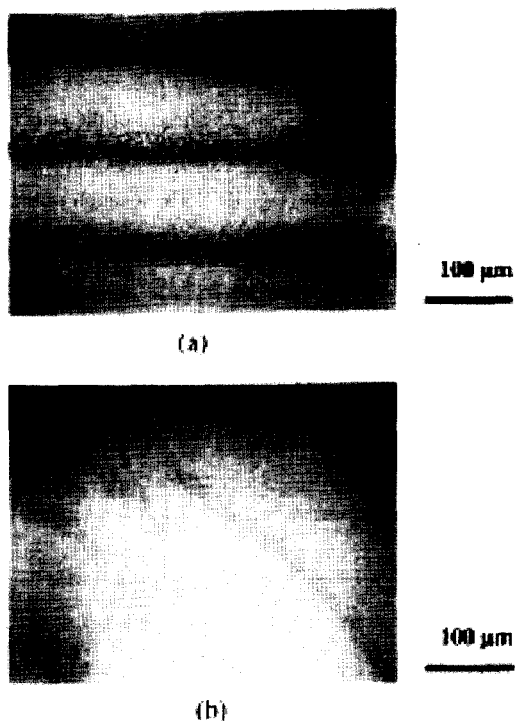


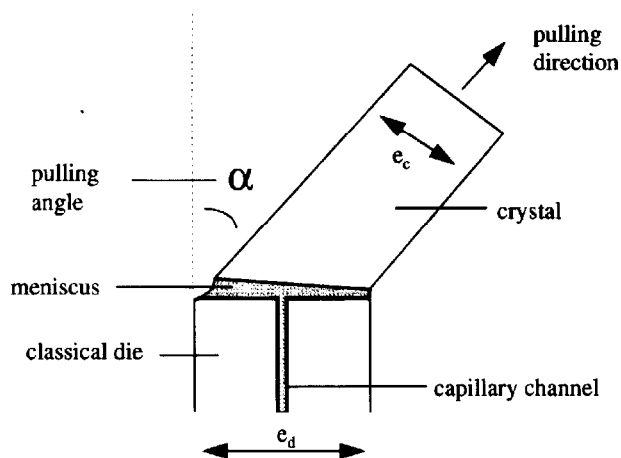
Fig. 21. Longitudinal sections of GES sapphire crystals using a 1 rpm rotation rate at a ratio  $V/\omega$  equal to: (a) 130  $\mu\text{m}$ ; (b) 4  $\mu\text{m}$ .

Light transmittance measurements along the  $C$ -axis are compared for GES samples with 4  $\mu\text{m}$  and 130  $\mu\text{m}$  layer thicknesses [45]. When the crystallized layer is small enough, the light transmittance for GES crystals become comparable with Gentilman's reference data [47].

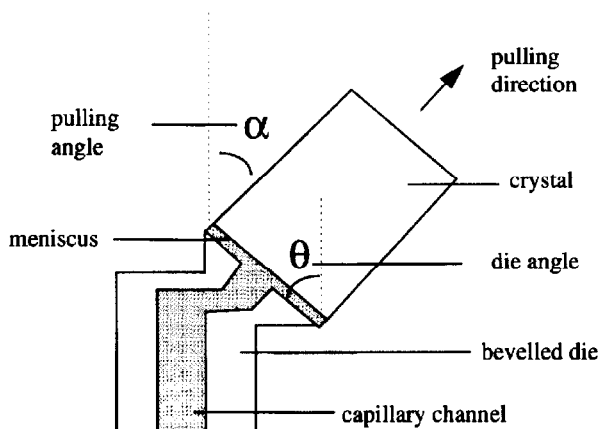
#### 4.2 Growth of near-net shaped dome crystals

The most difficult part of growth is the initial stage of hemisphere formation after seeding, when pulling is carried out practically only in a horizontal direction. The size of the crystal cross section  $d_c$  depends on the size of the die-top cross section  $d_d$  and the angle  $\alpha$  between the pulling direction and vertical axis; it is determined by a simple ratio  $d_c = d_d \cos \alpha$  for a horizontal die-top

surface, Fig. 22a. In the initial stage of growth the thickness of a hemisphere wall approaches zero and growth is impossible because of the absence of the attachment of the melt column to the die edge.



(a)



(b)

Fig. 22. Scheme showing the dependence between size of the die-top and crystal cross-sections for: (a) horizontal die-top surface, (b) tilted die surface.

An idea to solve this problem is to design the die with a tilted top surface [48], as shown on Fig. 22b, in order to make the process available for any crystal shape by rotation of the seed together with a combination of vertical and horizontal translations. A  $45^\circ$  tilted angle for the molybdenum die is optimum for use with a factor  $d_d/d_d = \sqrt{2}$  for pulling crystals over a wide range of angles.

The thickness of the growth layer per one turn of a die angle of  $45^\circ$  is:

$$h_c = \frac{V_x \cos \theta + V_z \sin \theta}{\omega},$$

where  $V_z$  and  $V_x$  are the corresponding vertical and horizontal translation rates, and  $\omega$  is the rotation rate.

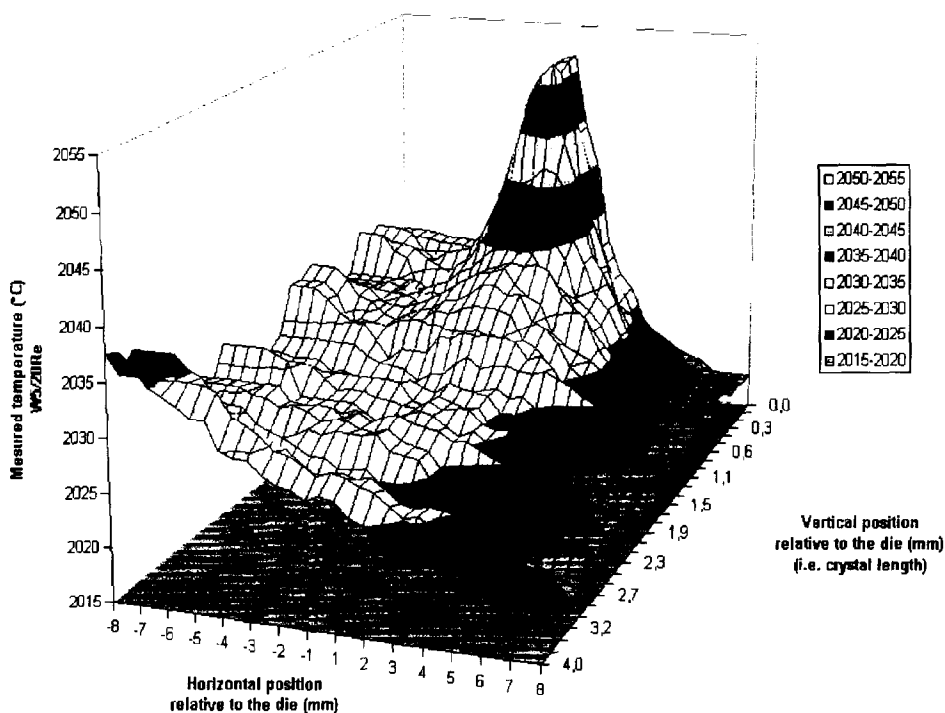


Fig. 23. *In situ* GDS temperature measurement during the growth of a ribbon. A thermocouple was attached to the seed.

#### 4.3 Critical strain rate criterion for crack-free dome growth

A failure mechanism is proposed in order to explain the generation and propagation of cracks during the growth of sapphire domes from an element of shape [49]. According to this model, 10  $\mu\text{m}$  gas bubbles expansion is induced by glide dislocations (Orowan's model), up to a critical size for which the crack is initiated. Numerical simulation of stresses during growth explains how cracks propagate first vertically (V-type cracks) then horizontally (H-type cracks). The calculations were done on the base of *in situ* temperature measurements [50]. Fig. 23 is a temperature recording of an immersed thermocouple (TC) translated from one side to the other of a growing GES ribbon. In order to avoid crack initiation, it is necessary to keep below the critical value of the plastic strain rate that relaxes the stresses and at the same time lengthens the initial defect. One solution consists in relaxing the opening hoop stress with the same efficiency as that which is lengthening the defect.

A criterion based on plastic strain relaxation is defined in order to determine the growth parameters (pulling and rotation rates) as a function of the measured thermal gradients in the crystal. The time derivative of the crystal base radius is the same as the horizontal translation rate of the seed,  $V_x$ ; a no failure criterion is obtained:

$$\omega(r) \leq \frac{\frac{2\varepsilon_{pl}^{\max}}{\alpha_{th}} - |V_x| \nabla_r T}{2\pi r \nabla_r T}.$$

The vertical translation  $V_z$  is combined with the other displacements to grow sapphire domes in the way presented in Fig. 24a.

According to the equation,  $\omega$  reaches its lowest value,  $\omega_k$ , at the end of the growth, where the crystal radius is a maximum. This defines the linear growth rate that is kept constant all along the process in order to keep a constant liquid flow rate in the die. In practice, crack-free crystals were obtained for linear pulling rates of about twice the latter critical value, a result consistent with the fact that the  $\sigma_{\theta\theta}$  stress component achieves its maximum when the crystal horizontal radius is close to half the ultimate base radius [49].

The other parameters ( $V_x$ ,  $V_z$ ) derive from the Pythagorean relation and from crystallised layers of constant thickness. In practice, ( $V_x$ ,  $V_z$ ,  $\omega$ ) are calculated at each time step, connected with latitude increments that describe the hemispherical dome from its top to its base. These increments ( $0.5^\circ$ ) are fine enough to get a roughness lower than the surface defect between successive growth layers.

This led to the growth of GES crack-free sapphire hemispheres, Fig. 24b, that can be used for infrared dome blanks.

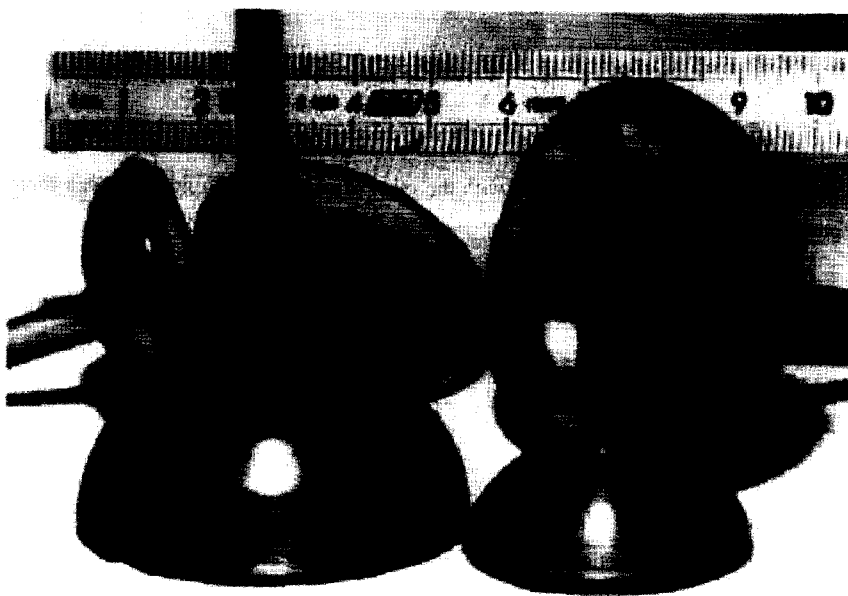
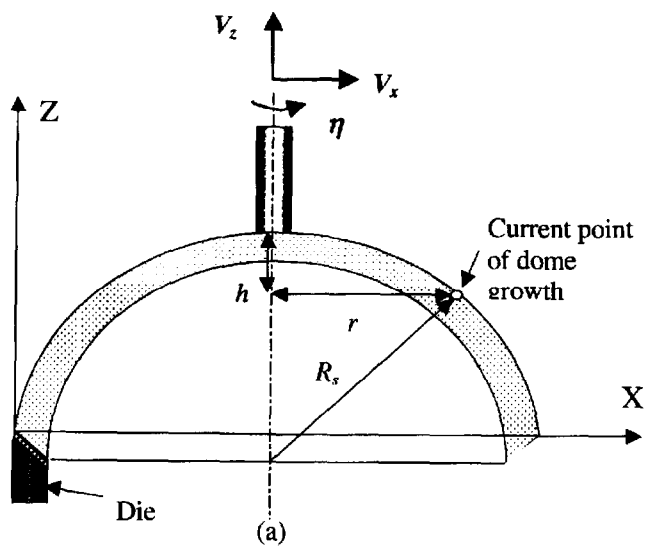


Fig. 24. Principle of the growth of a dome from an element of shape (a) and crack-free sapphire hemispheres (b).



## 5. Modulation-Doped Shaped Crystal Growth

### 5.1 Periodical doped structures

A current problem in the field of optoelectronics is the development of new materials that can combine in themselves several different functions simultaneously. One way to solve this problem is the growth of bulk crystals with regularly doped structures. In particular, the presence of spatial resonance structures (periodic structures of variable composition) in crystals of  $Al_2O_3:Ti^{3+}$  sharply reduces the threshold for laser oscillation and makes it almost independent on the outside cavity characteristics [51]. The characteristics of the laser medium are also influenced by the contrast of the spatial resonance structures in terms of a parameter  $a$ , for example, refractive index. The contrast is determined as in Equation, and at the same time is a function of many variable quantities (the activator concentration, the growth conditions, etc.).

$$K = \frac{a_{\max} - a_{\min}}{a_{\max} + a_{\min}}$$

As a model material we have used sapphire doped with active laser ions  $Ti^{3+}$ . As layer materials crystals grown by the Verneuil method have been used to contain no more than  $10^{-4}$  wt.% Ti in undoped layer material and up to 0.5 wt.-% in doped layer material. The doping contents in the grown crystals were measured using the X-ray microanalyzer “Camebax”. The modulation-doped structures in the grown crystals were observed using a scanning electron microscope DSN-960 (from Optron), the image contrast depending on the contents of the luminescent impurity  $Ti^{3+}$  in the matrix-activator pair.

#### 5.1.1 Obtaining periodic structures by the EFG technique

In the first variant for the *in situ* production of bulk crystals with regularly doped structures, crystals were grown by the EFG/Stepanov method in the shape of ribbons, rods, and tubes. The temperature fluctuations at the crystallization front can lead to the crystallization rate varying. Change of the crystallization rate leads to a periodic disturbance of conditions at the crystal-liquid interface and hence to periodic capture of the impurity by the crystal. The frequency of the temperature fluctuations can be varied by changing the pulling rates, periodic displacement of the dic, and by varying the power supply. The periodic change of the pulling rate was achieved in two different ways. Either the rate was periodically increased and decreased, or, the pulling mechanism was periodically

switched on and off. The duration of the periodic structures produced in this way ranged from 5 to 100  $\mu\text{m}$ . The periodic structure in a longitudinal section of a sapphire is shown in Fig. 25, [52]. The observation of dopant modulation in the grown crystals has been made using cathodoluminescence (scanning electron microscope DSN-960 (“Opton”)), the image contrast being dependent on the contents of the luminescent impurity in the matrix-activator couple.

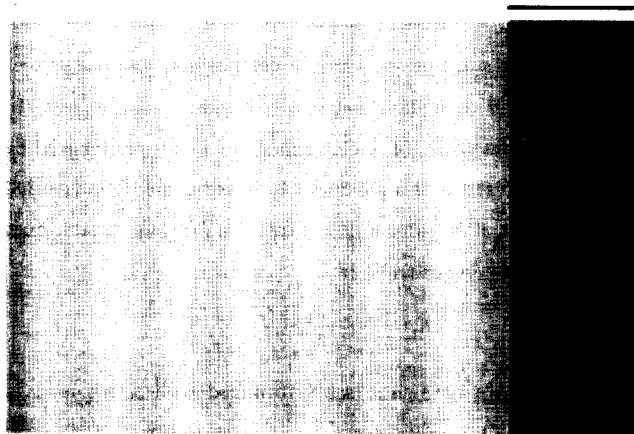


Fig. 25. The periodic structure in the longitudinal section of a sapphire rod grown by the EFG method. The structure was prepared by changing the pulling rate.

This approach also permits us to change the period of the spatially doped structures during the process of growth and to go from a periodically doped structure to a homogeneously doped structure [53].

The contrast in the stripes produced in the structures is not strong because it is limited by the redistribution of the impurity in front of the crystallization front in only a small volume of melt - in the meniscus. The activator concentration varies by no more than one order of magnitude. The thickness of the transition layer between “doped” and “undoped” regions is the comparable to the striation period. The contrast decreases with decreasing striation period and virtually vanishes for periods smaller than 5  $\mu\text{m}$ . Somewhat thinner transition layers were observed by periodically stopping the pulling.

### 5.1.2 Obtaining layered crystals by the GES technique

As is shown in Sec. 4, Antonov and his coworkers developed the GES concept by use of the simultaneous operation of two (or more) dies [39, 43]. The dies were placed at some distance from the rotation axis, the menisci form from small elements of the melt, Fig. 26a. Authors of these papers used layered single crystals having a composition  $\text{LiF-LiF:Mg}^{2+}$  as a model for the investigation of the mechanical parameters and dislocations in composite structures, Fig. 26b.

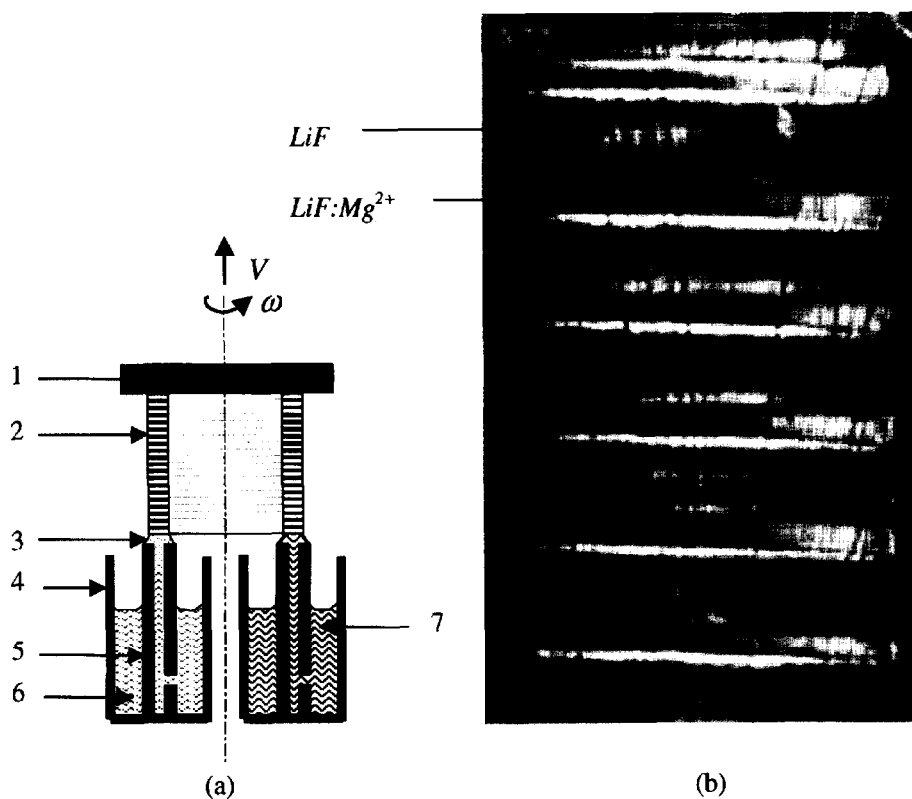


Fig. 26. GES method using two crucibles. (a) The scheme for layered crystal growth by the GES method : 1 – seed plate; 2 – layered crystal; 3 – meniscus; 4 – crucible; 5 – die; 6 – undoped melt; 7 – doped melt. (b) Photo of  $\text{LiF-LiF:Mg}^{2+}$  periodic structure.

Later, the applicability of the GES method for high-temperature multicomponent oxide crystal growth was investigated. Sapphire [52–54], calcium-niobium-gallium garnet (CNGG) and yttrium orthovanadate (YVO) [55] were chosen as representative test materials.

Shaped crystals in the form of rods and tubes were grown at a pulling rate of 3–25 mm/h and at a rotation rate 0.5–20 rpm. Grown crystals included regularly doped structures  $Al_2O_3 - Al_2O_3:Ti^{3+}$  with periods of 5–100  $\mu m$  [54], Fig. 27a. The impurity concentration in the undoped parts of the crystal was less than  $10^{-4}$  wt.% and in the doped parts of crystal was up to 0.2 wt%. The doped and undoped layers constitute spirals with the angle of the spiral line slope given by  $\alpha = \tan^{-1}(V/2\pi R\omega)$ , where  $R$  is the distance from the rotation axis of the seed holder to the axes of the dies (when dies are located at equal distance from the axis of rotation of the seed holder). The volume of the transition region between layers is defined mainly by the width of partial melting of the initially crystallized layer as a result of contact of the layer with the meniscus. The width of the partially melted zone and the character of the impurity distribution in the transition region depend on the thermal conditions in the crystallization zone, the frequency of rotation, and the pulling rate of the crystal. In particular, high contrast structures with a small period were produced under conditions close to supercooling on the crystallization front, that is with a small height of meniscus.

Application of the GES method lets us significantly develop the possibilities for the production *in situ* of various types of spatially periodic structures:

- A change of period during the growth process can be realized by variation of the relation  $V/\omega$  (Fig. 27b) [54].
- Application of this method allows one to predetermine the required ratio of layer heights within a period and also allows this ratio to be varied during the growth process, Fig. 27c [52]. Change of doped-undoped layer width ratio can be achieved by one of two ways, either by variation of the top surface level of one of the dies or by variation of the relative location of the dies in the case when the top surface levels are constant.
- Transition from the periodic structures to uniformly doped or undoped crystal was carried out by disconnecting melt feeding in one die during the growth process.
- Location of dies having various areas of work surface and/or various distances of dies from the rotation axis and/or combinations of the die's arrangement makes it possible to obtain various types of doping structures in crystals [54].

Fig. 27. Periodical structures of  $Al_2O_3 - Al_2O_3:Ti^{3+}$  grown by the GES method: (a) structure with constant period; (b) structure with a variable period; (c) structure with different ratios of width of doped and undoped regions in one period.

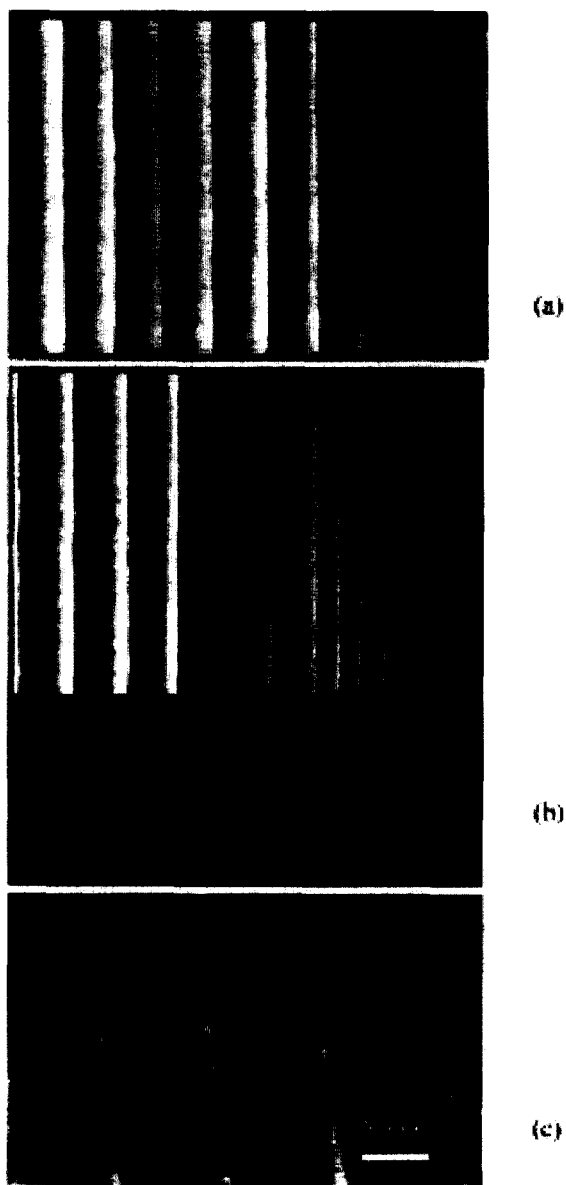


Fig. 27. Periodical structures of  $Al_2O_3 - Al_2O_3:Ti^{3+}$  grown by the GES method: (a) structure with constant period; (b) structure with a variable period; (c) structure with different ratios of width of doped and undoped regions in one period.

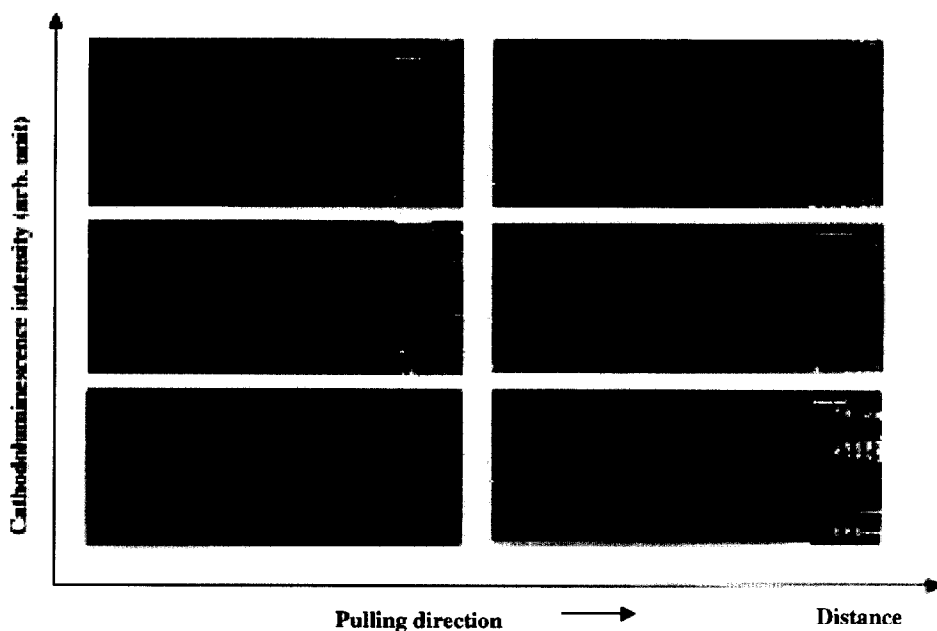


Fig. 28. The distribution of cathodoluminescence intensity (a. u.) along the  $Al_2O_3 - Al_2O_3:Ti^{3+}$  samples.

The two techniques of *in situ* preparation of the modulated structures described here can be used universally in the growth of crystals of other compositions from the melt. The structures in bulk crystals outlined above amount to a new class of materials. There is reason to believe that these structures will find applications in the development and fabrication of various devices.

### 5.2 Core-doped fibers

The availability of high-quality fiber crystals doped with active laser ions only in a sharply separated inner core region [56, 57] is of special interest. Because of the step-like change of the radial doping profile of non-linear optical core-doped fibers, the pumping energy is absorbed only by the central part and an efficient laser mode translation takes place.

For the first time Burrus and Stone [56] grew a thin ruby laser as a quasi-cladded core doped fiber with a diameter of 40  $\mu m$  by a two-step laser melting technique. Homogeneously doped ruby fibers were first grown by a floating-zone technique from small source rods, and then these fibers were

carefully surface melted in the same  $\text{CO}_2$  laser apparatus to outdiffuse the  $\text{Cr}$  in a region near the fiber surface. Such a structure had a modulated radial refractive index with improved waveguide properties, i.e. transmission efficiency.

For the first time core-doped fibers were grown directly from the melt by Dmitruk [58]. Two crucibles were combined with an outer and inner die for differently doped melts, Fig. 29. While the melt of the outer crucible rises only in a small central bore the melt of the inner crucible goes up within a ring-like aperture surrounding the central bore. A meniscus forms at the front consisting of two quasi different melt columns - an inner doped core and an outer undoped wrapping. Core-doped fibers of  $\text{CsBr}(\text{AgBr})\text{-CsBr}$  and  $\text{TlBr-TlBr}_x\text{Cl}_{1-x}$  compositions were grown.

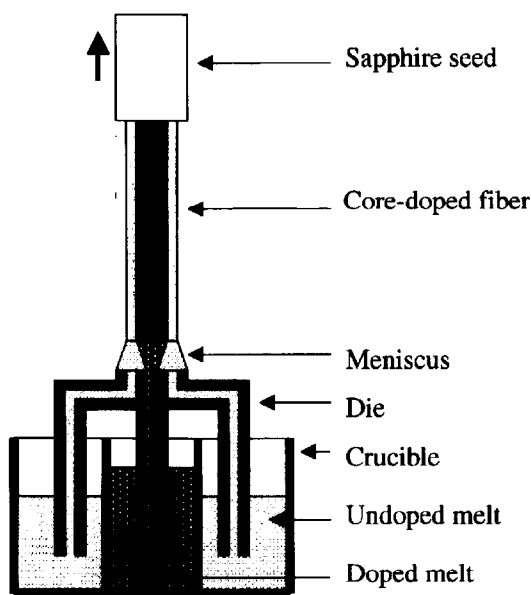


Fig. 29. Scheme for core-doped fiber growth using two crucibles.

Later, the same approach was used by Shimamura et al. [59] for  $\text{LiNbO}_3$  rods with a length of about 10 mm having an outer diameter of 5 mm consisting of a sharply separated inner  $\text{Cr}$ - or  $\text{Nd}$ -doped core region with diameters about 1.5 and 4 mm were successfully grown at pulling rates up to 60 mm/h.

Also this technique was used for preparing *in situ* of sapphire core-doped fibers ( $\text{Al}_2\text{O}_3 - \text{Al}_2\text{O}_3 : \text{Ti}^{3+}$ ) with automated weight control by Kurlov et al. [60].

To grow high-performance shaped crystals with different compositions in their cross-section it was necessary to solve the problem of the elimination of forced mass transfer across the meniscus between melts of various composition (the problem of “form”) and to control the introduction of gas bubbles and solid inclusions in the volume of crystal (the problem of “quality”).

In order to solve the first problem it is necessary to form and maintain a preset spatial component distribution in the meniscus and in the region of crystallization during the growth process, which is determined by thermal convection, mass exchange by diffusion and convection induced by a gradient of surface tension in the meniscus. The main parameters which determine the extent of mixing between the different melt compositions in the meniscus are the pulling rate, the meniscus height which is dependent on the thermal gradient, the geometric sizes of the capillary channels of the dies and the form of the die top. Calculations were carried out to estimate the spreading region of the core-doped part in the meniscus as a function of the pulling rate and the meniscus height with regard to diffusion in the meniscus:  $d_c = d_i + 2\sqrt{\frac{h_m D}{V}}$ , where  $d_c$  is the core diameter,  $d_i$  the diameter of the inner die bore,  $D$  the diffusion coefficient of the dopant in the melt,  $h_m$  the meniscus height and  $V$  the pulling velocity [57]. To grow a crystal with a small zone of mixing between the doped and undoped parts it was necessary to achieve a small meniscus height and large pulling rate simultaneously. This displaces the growth conditions at the crystallization front to the supercooling region. Supercooling is followed by the appearance of cellular structure and facets on the growth surface that results in the mass capture of bubbles and solid phase inclusions.

### 5.2.1 Automation as the source of high-quality core-doped fiber growth

In order to control the growth conditions at the crystallization front and prevent the formation of related defects an automated control system using a crystal weight sensor was applied to the process of shaped crystal growth. The principles of the control system and the means of measuring the conditions at the crystallization front in the growth process are described in detail in Ref. [61].

The meniscus height and the conditions at the melt-crystal interface, including supercooling and superheating, are closely related to the amplitude of the oscillations of the mass rate deviation  $\delta\dot{M}$ . Fig. 30 shows the cross-sections of fibers grown under different thermal conditions at the crystallization front and correspondingly under different amplitudes of  $\delta\dot{M}$ . These fibers 1.2 mm in diameter were grown using a pulling rate of 2 mm/min for a program mass rate of  $9 \cdot 10^{-3}$  g/min. A



core-doped fiber of high quality (Fig. 30 a, b) was achieved for  $\delta\dot{M}$  amplitudes in the range from  $\pm 0.03$  g/min to  $\pm 0.05$  g/min.

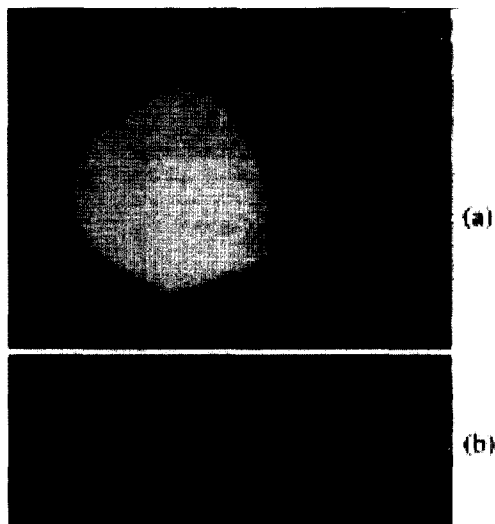


Fig. 30. The cross-section of a sapphire fiber grown at the optimum  $\delta\dot{M}$  amplitude (a) and distribution of the cathodoluminescence intensity corresponding to the content of the luminescence impurity (b).

Relatively large  $\delta\dot{M}$  amplitudes are connected with permanent noise in the melt-crystal system independently of the quality of the pulling mechanism. Conditions involving a superheated melt-crystal interface resulted in a smaller  $\delta\dot{M}$  amplitude (less than  $\pm 0.03$  g/min) for the same growth rate, Fig. 31. This resulted in the mixing of the doped and undoped melts in the meniscus. Conditions of supercooling at the melt-crystal interface resulted in a larger  $\delta\dot{M}$  amplitude (more than  $\pm 0.05$  g/min), see Fig. 32. During the first stage in the development of instability, involving values of  $\delta\dot{M}$  having amplitudes near  $\pm 0.05$  g/min, areas of cellular structure appeared on the smooth crystallization front which resulted in an increase in the probability of impurity capture, Fig. 32a. Then, as instability increased, the orientation of the cells developed singular forms. In the next stages the crystallization front became faceted which led to the mass capture of bubbles and solid-phase inclusions, Fig. 32b.

Depending on the analysis and selection of the  $\delta\dot{M}$  amplitude, control of the crystallization front condition could be achieved. In the process of the growth of variable composition fibers the

control was based on the maintenance of the amplitude of the  $\delta\dot{M}$  oscillation in a certain, very narrow, range of values to support the conditions at the melt-crystal interface close to the supercooling condition.



Fig. 31. The cross-section of a sapphire fiber grown under a superheating condition at the crystallization front.

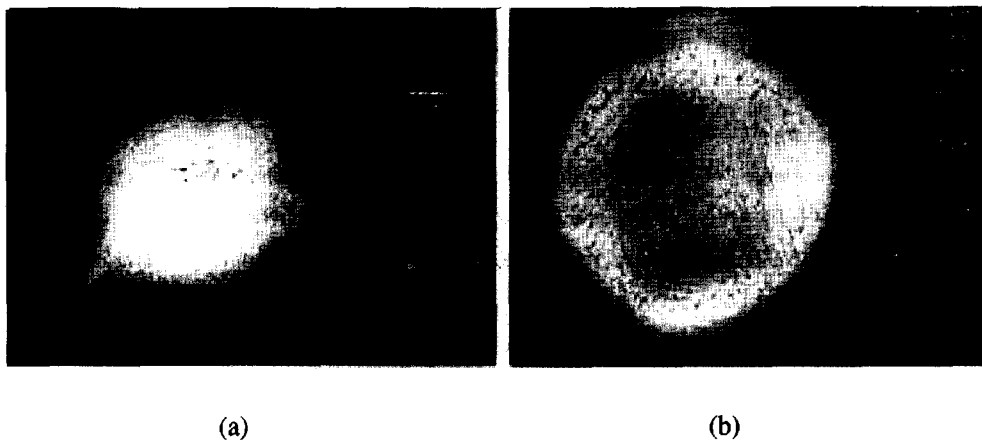


Fig. 32. The distribution of gas bubbles and solid inclusions in the cross-section of a sapphire fiber grown with supercooling at the crystallization front: (a) initial stage of cellular structure generation; (b) mass capture of inclusions resulting in the faceted crystallization front.

Supercooling at the crystallization front in the process of growing the variable composition crystals can be nonuniform because of constitutional supercooling in the zone of the more refractory melt, that results in the appearance of solid-phase inclusions in the doped part of crystal. To obtain the optimal distribution of temperature in the crystallization zone, the heights of the edge for the inside and outside parts of the die were varied.

### 5.3 Large composition-modulated shaped crystals

The modified EFG method involving two (or more) crucibles was also used to grow large composition-modulated  $Al_2O_3 - Al_2O_3 : Ti^{3+}$  [62] in the shapes of ribbons, tubes, and rods. One variant of the melt path designed for growing ribbons with a specific dopant distribution is presented in Fig. 33a. An as grown  $Al_2O_3 - Al_2O_3 : Ti^{3+}$  ribbon obtained with use of this die is shown in Fig. 33b. Fig. 34 shows various dopant distributions available with this modified EFG technique and the longitudinal section of an  $Al_2O_3 - Al_2O_3 : Cr^{3+}$  tube.

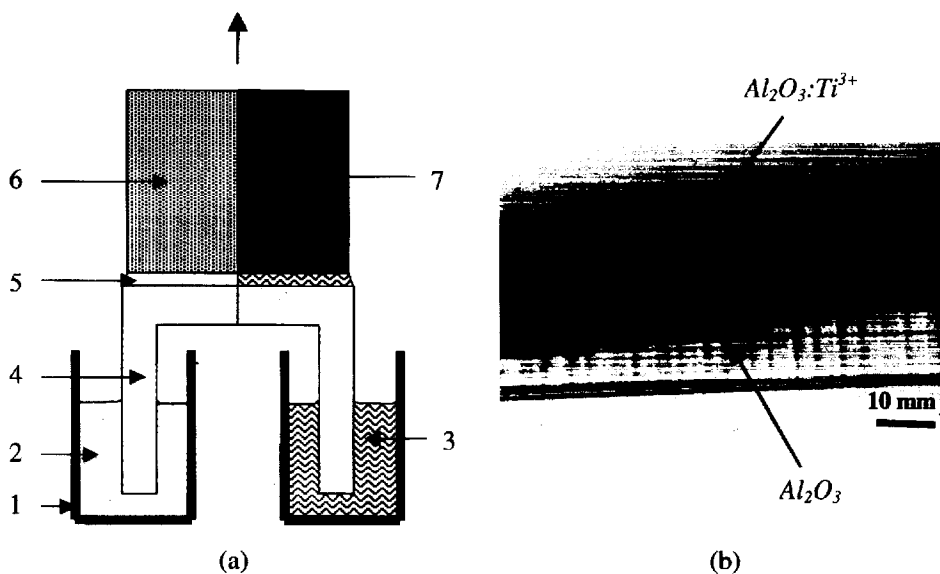


Fig. 33. Composition-modulated ribbon. (a) Schematic of pulling a composition-modulated ribbon: 1 – crucible; 2 – undoped melt; 3 – doped melt; 4 – die; 5 – meniscus; 6 – undoped part of ribbon; 7 – doped part of ribbon. (b) As-grown ribbon obtained on this scheme.

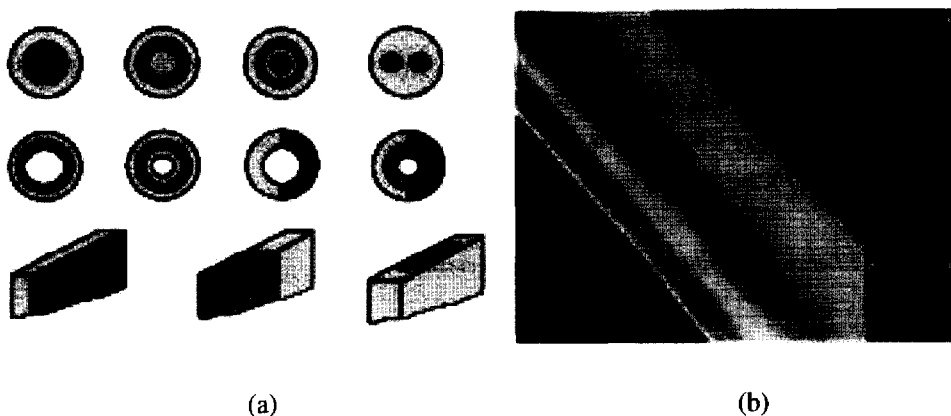


Fig. 34. Composition-modulated shaped crystals: (a) transverse dopant distribution in rods, tubes, and ribbons obtained by the modified EFG method; (b) longitudinal section of the wall of a composition-modulated tube.

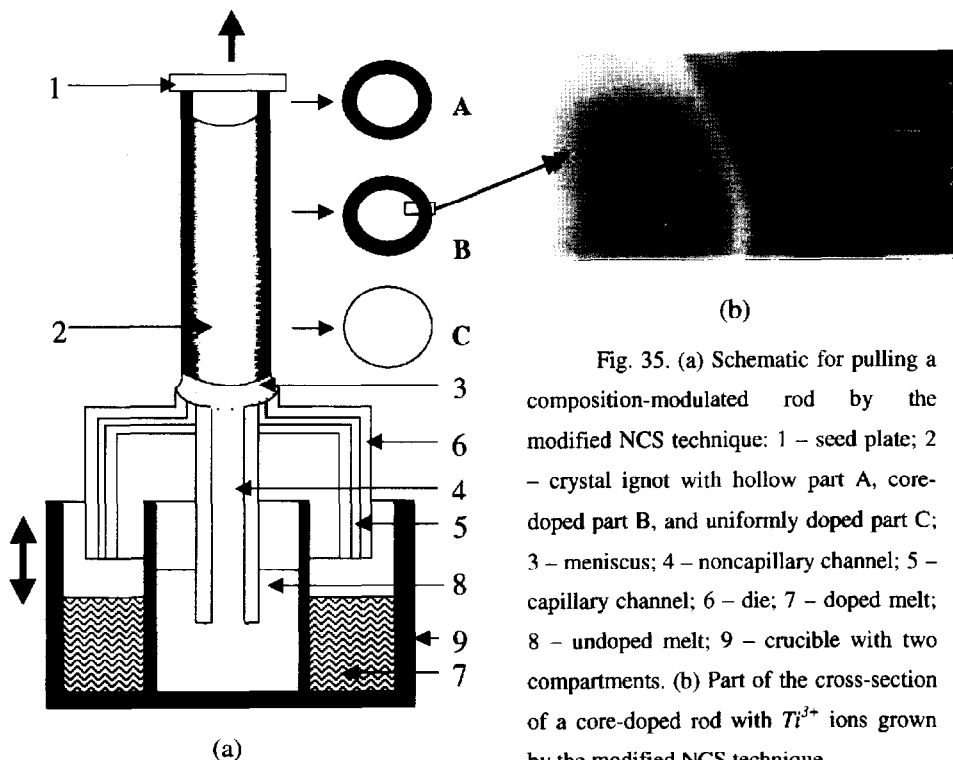


Fig. 35. (a) Schematic for pulling a composition-modulated rod by the modified NCS technique: 1 – seed plate; 2 – crystal ignot with hollow part A, core-doped part B, and uniformly doped part C; 3 – meniscus; 4 – noncapillary channel; 5 – capillary channel; 6 – die; 7 – doped melt; 8 – undoped melt; 9 – crucible with two compartments. (b) Part of the cross-section of a core-doped rod with  $Ti^{3+}$  ions grown by the modified NCS technique.

Also the modified NCS (see Sec. 3) technique was used for the growth of sapphire crystals of large cross-section with a controlled dopant distribution. Fig 35a [62] illustrates the transition from a core-doped rod (B) to a uniformly doped rod (C) which was achieved by switching off the melt supply through the capillary channel. The state of the crystallization front was controlled in such a way as to prevent the entrapment of solid and gaseous inclusions. The automated control system was similar to that used in the EFG technique (see Sec. 6).

The modified NCS method allows one to grow rods with various cross-sectional shapes and various transverse dopant distributions, thick tubes, and crystals of intricate external shape and doping patterns. Part of the cross-section of a 16 mm diameter rod core-doped with  $Ti^{3+}$  ions is shown in Fig. 35b.

## 6. Shaped crystal growth using automated weight control

Gas bubbles, solid-phase inclusions and grain boundaries are widely known defects in shaped crystals. They sharply degrade the optical and mechanical properties of the material. One of the most probable reasons for their appearance is supercooling at the melt-crystal interface (thermal or constitutional supercooling). As a result of the supercooling, the crystal growth process becomes unstable [63–67].

Instability of the crystallization front results in the intensive capture of impurities, inclusions and gas bubbles and, therefore, in the low quality of the crystal structure.

By convention one can characterize four stages of supercooling at the melt-crystal interface exist with regard to their influence on crystal quality:

(1) Appearance of separate areas of cellular structure resulting in an increase in the probability of inclusion capture.

(2) Appearance of facets on the crystallization front resulting in mass capture of inclusions and the generation of grain boundaries.

(3) Additional supercooling and a marked decrease in the meniscus height will cause interaction between the crystallization front and the working surface of the shaper causing a distortion of the growing crystal, i.e. in an undesirable change of the crystal shape.

(4) The last stage of additional supercooling results in freezing of the crystal to the shaper and shaper damage.

Visual observation and manual control enables the crystal grower to identify the situation and make corrections only at stages (3) and (4). Visual observation and manual control are especially difficult during multi-crystal growth and during the pulling the crystals of complicated shapes. Besides

the manual regulation of crystal shape, it is necessary to control the quality of the growing crystal by changing the melt-crystal interface position. Visual observation is difficult even during single sapphire crystal growth because of the very small meniscus height and the similar brightnesses of the meniscus and crystal near the interface boundary. So, it is impossible to control manually the position of the crystallization front at stages (1) and (2).

In order to control conditions at the crystallization front and prevent the formation of growth defects it is worth while applying an automated control system using a crystal weight sensor in the process of shaped crystal growth.

Direct application of an automated control systems such as that developed for the Czochralski technique is unacceptable in the case of shaped sapphire growth because of anchoring of the meniscus to the edge of the die. This additional constraint for the growth of shaped sapphire is the essential difference to the Czochralski technique.

The principles of automated control of shaped crystal growth with the use of a crystal weighing technique have been developed [61] for the first time for all stages of the pulling process (seeding, crystal enlargement, stationary growth, *in situ* cross-section changing). Automated computer systems provide the *in situ* crystal quality control as well as the crystal shape control, which allows one to increase the output of high-quality crystals and to expand the areas of applications of sapphire crystals for device structures and as an optical material.

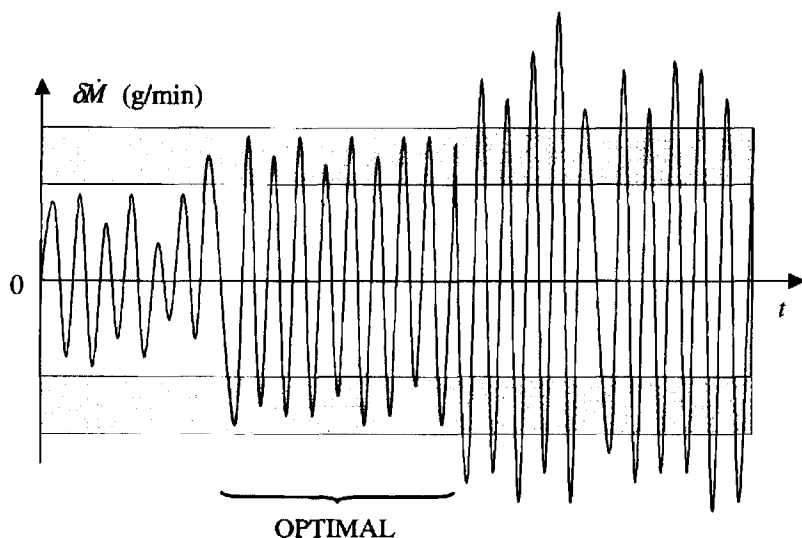
Regulation of the crystal cross-section was achieved by controlling the deviation  $\delta M$  of the real mass  $M_r$  from the program mass  $M_p$  by variation of the heating power  $P$ . The real mass  $M_r$  is calculated from the measured weight signal  $W$ .

The meniscus height and the conditions at the melt-crystal interface, including supercooling and superheating, are closely related to the amplitude of oscillations of the deviation of the mass rate  $\delta \dot{M}$ . The amplitude of the oscillations  $\delta \dot{M}$  corresponds implicitly to the meniscus height and the position of the melt-crystal interface. A relatively small amplitude of  $\delta \dot{M}$  indicates superheating of the melt-crystal zone and a rather large meniscus height. This may result in the appearance of facets on the lateral surface of the growing crystals with a decrease of their cross-section and further a subsequent rupture of the meniscus. The upper boundary of the  $\delta \dot{M}$ -amplitude is the most important parameter for automated growth of shaped crystals of high quality. A large  $\delta \dot{M}$ -amplitude corresponds to supercooling in melt-crystal zone, i.e. the meniscus height is correspondingly small. In this case the cellular structure can be formed on the melt-crystal interface, which leads to the formation of defects in the growing crystal. A further increase of the amplitude  $\delta \dot{M}$  may lead to the

partial freezing of the crystal to the die and to an undesirable change of crystal shape. The meniscus becomes so small that the crystallization front “sits down” on the working surface of the shaper.

In the monograph of Tatarchenko [68] the degree of stability of the crystallisation process was defined as  $\min [ |ReS_1|, |ReS_2| ]$ , here  $|ReS_i|$  is the absolute value of the real part of the root  $S_i$  ( $i=1,2$ ) of the second order characteristic equation of the “melt-crystal” dynamic model. As a smaller relative difference occurs between the melt and the crystallisation temperature a condition (“colder” meniscus) develops which corresponds to a smaller degree of stability. Thus the growth of a crystal in the “cool” regime is achieved with a smaller degree of stability. It also leads to a decrease of the phase and an amplification of the margin of stability of the automatic control system if the regulating parameters are not changed during the growth run. The oscillation mode in the weight and heating power signal practically always exists, with variable frequencies and amplitudes, as a reaction to thermal disturbances in the “melt-crystal” system and as a consequence of the closed loop structure. A decrease in the margin of stability results in the amplification of the oscillation mode and with a corresponding increase in the amplitude of the  $\delta\dot{M}$  oscillations.

Control of the crystallization front condition could be achieved through analysis of the  $\delta\dot{M}$  amplitude was realized. In the process of shaped crystal growth control was based on the maintenance of the amplitude of the  $\delta\dot{M}$  oscillation to a certain, very narrow, range of values that supported the optimum growth conditions at the melt-crystal interface, Fig. 36. For stationary growth the program mass rate  $\dot{M}$  is constant, and depends on the cross-sectional area of crystal. The proportional-integral-differential (PID) procedure relating to  $\delta\dot{M}$  was used in the closed-loop for the automated system. The change of the heating power during control resulting from PID processing of the deviation  $\delta\dot{M}$  was limited to a certain value  $|\delta P|_{\max}$ . The geometrical parameter  $r$  of the crystal (e.g. radius of the rod or thickness of ribbon, tube) involved in the calculation of the program mass and thus in the evaluation of the deviation  $\delta\dot{M}$  as well as heating power limitation  $|\delta P|_{\max}$  were the main parameters influencing the  $\delta\dot{M}$  amplitude and its maintenance over a certain range. The automatic evaluation of the geometrical parameter  $r$  from the weight signal was obtained from the controlling software during the growth run. So, the user has the possibility to evaluate the parameter  $r$  and to change its program value  $r_p$  without an interruption to the process control. The geometrical parameter  $r$  is the main parameter for changing the  $\delta\dot{M}$  amplitude in the necessary range. Varying  $r$  changes the mean value of the  $\delta\dot{M}$  oscillations and thus changes the slope of the heating power curve. This results in superheating or supercooling of the meniscus at the melt-crystal interface, and the  $\delta\dot{M}$  amplitude respectively decreases or increases.



36. Schematic amplitude of the  $\delta \dot{M}$  oscillation during shaped crystal growth.

The value of the heating power limitation  $|\delta P|_{\max}$  also influences the character of the heating power curve. A sufficiently small value of  $|\delta P|_{\max}$  results in an increase of the auto-oscillations in the heating power (in our case of its permanent increase during the growth run) and, consequently, in larger oscillations of  $\delta \dot{M}$ , i.e. in the supercooling regime. Larger  $|\delta P|_{\max}$  leads to greater freedom in the closed-loop and to more accurate portions of power change at each step of control and to a smaller of amplitude  $\delta \dot{M}$ . Therefore, variation in the limitation  $|\delta P|_{\max}$  during the growth process was also used for the changing the  $\delta \dot{M}$  amplitude under constant and optimum growth parameters of the PID controller.

But sometimes it is necessary to change the parameters of the PID procedure, namely, its integral coefficient (integration time). The value of total heating power change during the whole process depends on the dimensions of the crystal profile. The greater the profile of the crystal, the greater is the total power change in our case. Larger necessary power change requires a larger integral part in the PID "mixture" to provide the same, sufficiently small, regulation error.



### 6.1 Process of automated crystal seeding

The crystal seeding is an important stage of the growth process. The further stages of crystal growth depend on successful seeding. So, the seeding process has found its own place in the general problem of automatization of sapphire crystal growth.

Fig. 37 shows a simplified algorithm scheme for the process of automatic seeding which shows the logical connections between the main stages of the seeding process.

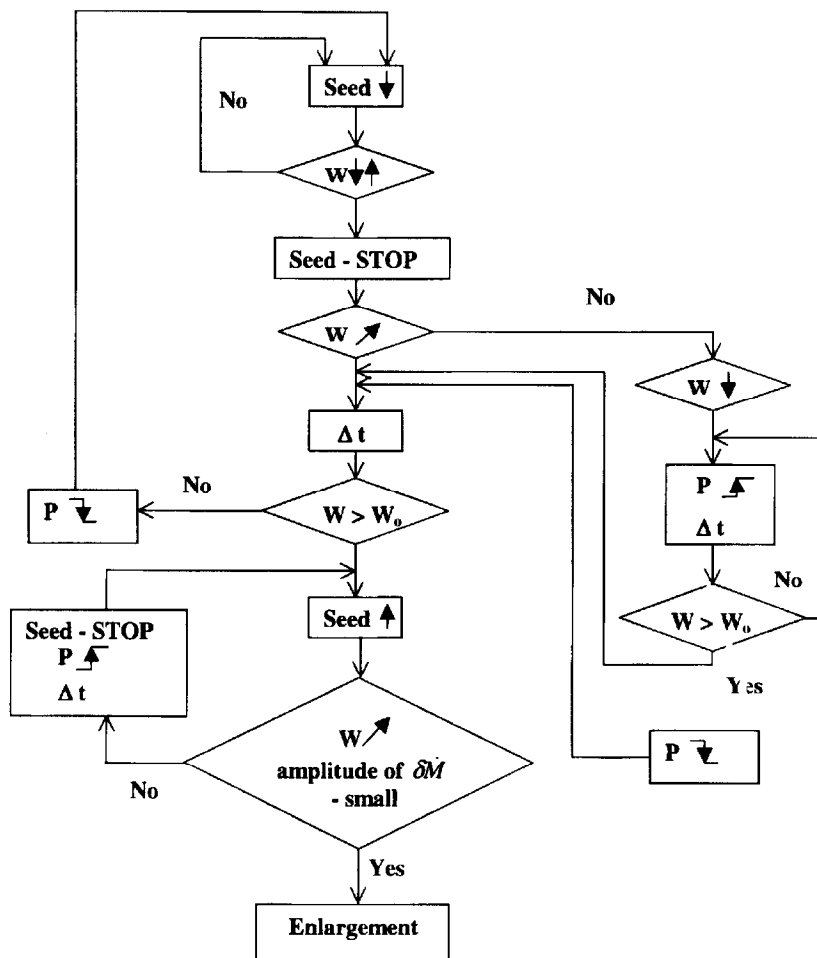


Fig. 37. A simplified algorithm scheme for the process of automatic seeding.

There are two main versions of the seeding procedure. In the first case the seed crystal partially melts, which results in a sufficiently slow increase of the weight signal  $W$ . The value of the weight signal change is proportional to the area of seeding. The weight signal increase can be explained by the influence of the surface tension force on the weight signal. The surface tension force appears when the seed starts to melt, and this results in the melt meniscus formation between the seed and the shaper. Too extensive seed melting may result in the rupture of the meniscus and a sharp decrease of the weight signal. In case of the meniscus rupture the heating power is decreased automatically by a certain value, and the seeding process is to be repeated. This “calculation-technological” cycle is repeated until the weight signal increases slowly or decreases (after its slow increase because of the meniscus formation) down to the value which is not less than that before the seeding cycle.

In the second case the “cold” contact of the seed crystal and shaper occurs (without meniscus formation) and the weight signal  $W$  decreases sharply. After that the heating power will be increased step by step until meniscus formation starts.

The process of the automatic crystal seeding is tuned by a certain set of software parameters to get a stable “calculation-technological” iteration process. The most important parameters which influence the stability of crystal seeding process are as follows:

- maximum rates of seed crystal lowering and lifting;
- minimum time interval of the evaluation of the weight data change;
- minimum time interval for melt exposure under a certain value of heating power;
- minimum step in the heating power change.

The crystal pulling starts when the controlling computer has “understood” that crystal seeding was successfully achieved. Crystal expansion proceeds if the weight signal  $W$  increases gradually with a sufficiently small  $\delta\dot{M}$ -amplitude. The absence of a gradual increase of the weight signal or too large a  $\delta\dot{M}$ -amplitude at the first moments of crystal pulling indicate supercooling in the melt-crystal zone. In this case the computer will automatically increase the heating power until the weight signal starts to grow gradually with a sufficiently small  $\delta\dot{M}$ -amplitude, and then the process of crystal expansion will begin.

## 6.2 Crystal enlargement

The enlargement is also a very important stage for shaped crystal growth, especially in the case of large-scale crystal growth. For automated shape control the relationship between the preset shape of the crystal and the program weight data change should be known for each moment of time.

The program mass change includes the changes of crystal and meniscus mass and the influence of the surface tension force of the meniscus. The larger the contour of meniscus anchoring the greater is the surface tension influence on the weight signal.

We consider a non-dimensional parameter  $P = \frac{S}{aL}$ , characterizing indirectly the ratio of the weight force to the force of surface tension.

Here  $S$  is the summation area of the anchoring contours,  $L$  is the summation length of these contours,  $a$  is a capillary constant. The influence of the force of surface tension of the meniscus on the weight signal is sufficiently large when  $P < 1$ . For example, for a tube growing by the Stepanov technique and having the wall thickness  $\delta_T$  this ratio is equal to  $P = \frac{\delta_T}{2a}$ . In many processes of thin wall tube growth  $P < 1$ , so it is important to take into account the influence of the surface tension force.

For the accurate consideration of this force many parameters such as the density  $\rho_L$  of the melt, the liquid-gas surface tension coefficient  $\sigma_{LG}$ , the geometry of the die under the high temperature of the melting zone, the shape of the melt-crystal interface, the angles of the anchoring of the meniscus to the edges of shaper must be known with a high degree of accuracy. Calculation of the program mass for various profiles is not complicated and can be determined by integrating the preset crystal shape. The cases for ribbon [69], tube (one point [61, 70] and two point seeding [70]) enlargement have been reported.

Since the meniscus parameters can not be calculated exactly during the growth process, especially for complicated cross-sections of crystals and multi-crystal processes, it is difficult to describe exactly the program mass change. For the compensation of error for this calculation one parameter of the meniscus is corrected from the measured weight signal with the other “doubtful” parameters of meniscus and crystal being constant. Therefore, one parameter involved in the equations for the mass  $M_s$  of solidification fraction and the mass  $M_l$  of the meniscus is adjusted in order to compensate the estimation errors of the other parameters. For this selected parameter an equation can be solved.

### 6.3 Achievement of automated control

Various techniques have been used and different crystal profiles grown to illustrate the functioning of automated control systems.

The main problems which have been solved in the growth experiments using the automated control systems are:

- increase of crystal quality;
- growth of large-scale crystals;
- increase in productivity of the crystal growth processes by means of the multi-crystal growth techniques;

Large-scale sapphire single crystals such as tubes of large diameter, ribbons, rods with complicated cross-section, rods with capillary channels, etc. have been grown by the EFG/Stepanov method by using the automated control system. Rods, tubes with thick walls, and near-net-shaped sapphire domes have been grown by the NCS technique using automated control.

A serious problem in the design of the melting zone exists in processes for large-scale crystal pulling. Large dimensions of the window for observation of the melting zone make the thermal conditions of the crystallization process worse and is one of the reasons for the appearance of strong thermal stresses in the growing crystals. The automated control system enables the production of the sapphire crystals almost without use of the viewing window, and it simplifies the problem of the thermal zone design for large-scale crystal growth. A small viewing window is necessary only in the initial stages of crystal expansion.

Sapphire tubes with diameter up to 85 mm (Fig. 38) [70] and ribbons of 120 mm in width for optics, Fig. 39, [69] have been grown using the automated control system.

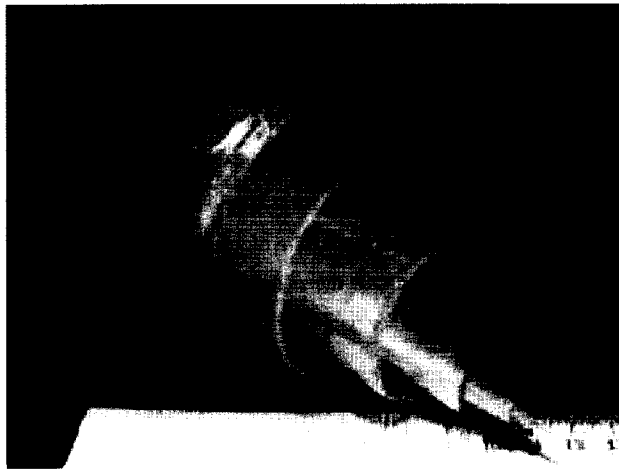
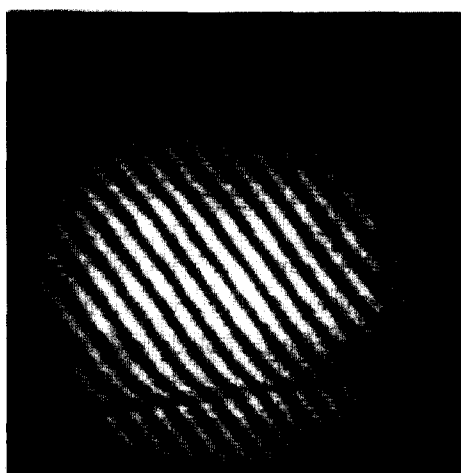


Fig. 39. Sapphire ribbon of 120 mm in width which have been grown using an automated control system (a). Interferogram of a polished plate 6 mm thick (b).



(a)



Edge of the plate

(b)

Fig. 39. Sapphire ribbon of 120 mm in width which have been grown using an automated control system (a). Interferogram of a polished plate 6 mm thick (b).

A multi-run pulling process with *in situ* quality control provides an increase in growth productivity. Sapphire crystals in the shape of the rods with up to 50 crystals per one process were grown by a multi-run pulling process, Fig. 40. The sum total length of crystals grown in one process reached more than 60 m. The diameter deviation was not more than  $\pm 0.1$  mm, misorientation between the grain boundaries was not more than  $2\text{--}3^\circ$  over a maximum length of 1300 mm.



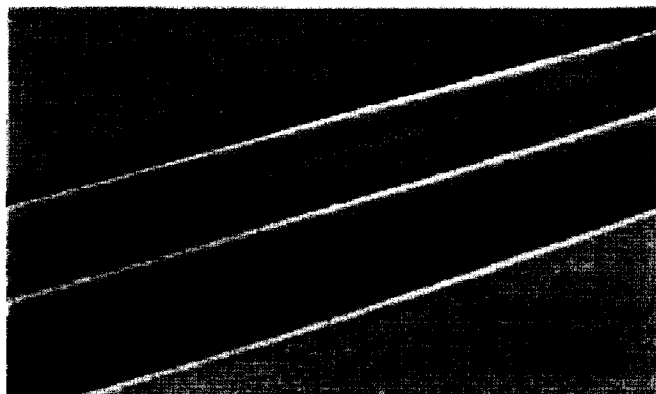
Fig. 40. Sapphire crystals grown by multi-run pulling process (rods 3.0 mm in diameter and tubes 3.5 mm in outer diameter).

It was interesting to apply automated control to the growth of sapphire rods with one or several channels of small diameter (less than 0.7 mm). This diameter is significantly less than the sapphire capillary constant. Growth of such crystals is very difficult because of the high probability of filling the channels with melt. In this case the growth of high quality crystal is possible only over a small pulling range rates whilst maintaining a small height of meniscus. The state of the melting zone while the pulling these crystals is close to a condition of supercooling. The use of automated control in this case is based on the maintenance of the mass rate deviation  $\delta\dot{M}$  over a certain range of values. The lower limit of the  $\delta\dot{M}$ -amplitude is defined by the possibility of filling the channels with melt, and the upper limit of the  $\delta\dot{M}$  oscillations depends on the expansion of the channels and the freezing of the crystal to the shaper.

A small range of  $\delta\dot{M}$  oscillations and a small height of the meniscus result in a decrease of the rates of convective flows in the meniscus and create the condition of meniscus anchoring to the edges of very small holes in the shaper. Successful growth of the sapphire crystals with small channels was possible due to the developed principles of the automated maintenance of the  $\delta\dot{M}$ -amplitude over a very small range. Sapphire rods 50 cm in length and 4.7 mm in diameter comprising five channels 0.6 mm in diameter and sapphire plate with channel 0.5 mm in diameter grown using an automated control system are shown in Fig. 41. Analogues principles are used for fiber growth with core-doped regions (see Sec. 5.2.1).



(a)



(b)

Fig. 41. The sapphire rods 4.5 mm diameter comprising 5 and 4 channels 0.6–0.7 mm in diameter (a). The sapphire ribbon comprising channel 0.5 mm in diameter (b).

The use of automated control in the NCS method is also important for all stages of crystal pulling (seeding, cross-section changing, stationary growth). Sapphire rods up to 40 mm in diameter, thick wall tubes and crucibles without gaseous inclusions in the volume of crystal and near-net-shaped sapphire dome blanks for high temperature optics have been produced by the NCS method using of the automated control system.

## 7. Conclusions

Sapphire has been produced commercially for many years and its unique properties make it an ideal material for hundreds applications. Despite the fact that sapphire has been used for many years, it is still in a stage of development. Optimization of standard crystal growth technologies and development of new techniques are actively pursued in order to increase the dimensions of crystals, improve the quality, reduce the cost of material, and to grow complex shapes. There are good reason to believe that sapphire will not only strengthen its position in traditional markets, but will also be used in a number of new applications.

## Acknowledgments

Authors wish to acknowledge Dr. S.N. Rossolenko, Dr. V.M. Krymov, Dr. P.A. Gurjiyants, Dr. S.V. Belenko, L.L. Kuandykov for helping and useful discussions during the preparations of this review. We also wish to thank Prof. J.B. Mullin for his valuable advice and corrections, which have greatly improved this review.

## References

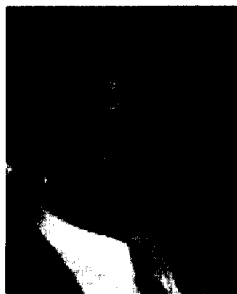
1. A.V. Stepanov, *Zh. Tech. Fiz.*, v. 29, 1959, p. 382 (in Russian).
2. A.L. Shach-Budagov, A.V. Stepanov, *Zh. Tech. Fiz.*, v. 29, 1959, p. 394 (in Russian).
3. A.V. Stepanov, *The Future of Metalworking* (Lenizdat, Leningrad, 1963) (in Russian).
4. S.V. Tsivinskii, A.V. Stepanov, *Zh. Tech. Fiz.*, v. 7, 1965, p. 194 (in Russian).
5. Yu.I. Koptev, A.V. Stepanov, *Fiz. Tverd. Tela*, v. 9, 1967, p. 3007 (in Russian).



6. Bulletin of the Academy of Sciences of USSR, Physical series: v. 33, No 12, 1969; v. 35, No 3, 1971; v. 36, No 3, 1972; v. 37, No 11, 1975; v. 40, No 7, 1976; v. 42, No 9, 1980; v. 44, No 2, 1980; v. 47, No 2, 1983; v. 49, No12, 1985; v. 52, No 10, 1988; v. 58, No 9, 1994; v.63, No 9, 1999.
7. Proceedings of Stepanov Conference, Ioffe Physico-Technical Institute, Leningrad, 1968, p. 209; 1989, p. 276. (in Russian).
8. “Shaped Crystal Growth” (Editors G.W. Cullen, T. Surek and P.I Antonov) in *J. Crystal Growth*, v. 50, 1980.
9. Proceedings of SSCG-1 in *J. Crystal Growth*, v. 82, No1/2, 1986.
10. Proceedings of SSCG-2 in *J. Crystal Growth*, v. 104, No1, 1990.
11. P.I. Antonov, L.M. Zatulovskii, A.S. Kostigov, D.I. Levinzon, S.P. Nikanorov, V.V. Peller, V.A. Tatarchenko, V.S. Yuferev, Editors: V.R. Regel, S.P. Nikanorov, “The growth of shaped single crystals and industrial articles by Stepanov method.”, Leningrad, Nauka, 1981, p. 280. (in Russian).
12. V.A. Tatarchenko “Shaped Crystal Growth”, Kluwer Academic Publishers, Netherlands, 1993, p. 287.
13. P. Rudolph “Profile Crystal Growth” (in German), Akademie Verlag, Berlin, 1982.
14. T.F. Ciszek, *J. Crystal Growth*, v.66, 1984, p. 655.
15. Yu.N. Buzynin, A.N. Buzynin, N.I. Bletskan, A.Yu. Malinin, E.B. Sokolov, *Elektronnaja Tehnika, Serija Materialy*, is. 10, 1977, p. 3 (in Russian).
16. P.I. Antonov, S.I. Bakholdin, S.P. Nikanorov, *Progress in Crystal Growth and Characterization of Materials*, v. 16, 1988, p. 19.
17. P. Rudolph, T. Fukuda, *Cryst. Res. Technol.*, v. 34, No 1, 1999, p. 3.
18. H.E. LaBelle, Jr., A.I. Mlavsky, *Nature*, v.216, 1967, p. 574.
19. A. Mlavsky, N.A. Panidscic, 1975, US Patent, No. 3868228.
20. H.E. LaBelle, C. Cronan 1975, US Patent, No. 3915662.
21. D.Ya. Kravetskii, L.P. Egorov, L.M. Zatulovskii et al., *Bull. Acad. Sci. USSR, Phys. Ser.*, v. 44, 1980, p. 126.
22. L.M. Zatulovskii, D.Ya. Kravetskii, L.P. Egorov, et al. *Bull. Acad. Sci. USSR, Phys. Ser.*, v. 47, 1983, p. 157.
23. V.A. Borodin, T.A. Steriopol, V.A. Tatarchenko, T.N. Yalovets, *Bull.Acad. Sci. USSR, Phys. Ser.*, v. 47, 1983, p. 151.
24. V.A. Borodin, T.A. Steriopol, V.A. Tatarchenko, *Cryst. Res. Technol.* v. 20, 1985, p. 833.
25. V.A. Borodin, V.V. Sidorov, S.N. Rossolenko, T.A. Steriopol, T.N. Yalovets, *J. Crystal Growth* v. 198/199, 1999, p. 201.
26. W.A. Tiller, K.A. Jackson, J.W. Rutter, B. Chalmers, *Acta Met.*, v. 1, 1953, p. 428.

27. Ya.E. Geguzin, A.S. Dzyuba, N.V. Kononenko, *Kristallografiya*, v. 26, 1981, p. 571.
28. S. Miyazawa, *J. Crystal Growth*, v. 49, 1980, p. 515.
29. J.P. Kalejs, *J. Crystal Growth*, v. 44, 1978, p. 329.
30. H.E. LaBelle, *J. Crystal Growth*, v. 50, 1980, p. 8.
31. V.A. Borodin, T.A. Steriopo, V.A. Tatarchenko, T.N. Yalovets, *Cryst. Res. Technol.*, v. 20, 1985, p. 301.
32. E.P. Andreev, L.A. Litvinov, V.V. Pischik, *Proc. All-Union Conf. On the Production of the Shaped Crystals and Products by the Stepanov Method and their Applications in the Nation Economy (LIYaF, Leningrad, 1986)* p.87 (in Russian).
33. V.N. Kurlov, *Bull. Rus. Acad. Sci., Ser. Phys.*, v. 58, 1994, p. 5.
34. V.N. Kurlov, *J. Crystal Growth*, v. 179, 1997, p. 168.
35. V.A. Tatarchenko, in: *Handbook of Crystal Growth*, Ed. D.T.J. Hurle (Elsevier, Amsterdam, 1994) p.1011.
36. P.I. Antonov, S.I. Bakholdin, M.G. Vasiljev, V.M. Krymov, V.S. Yuferev, *Bull. Acad. Sci. Ser. Phys.*, v. 52, No 10, 1988, p. 1997.
37. I.V. Alab'ev, S.V. Artemov, V.S. Papkov, V.F. Perov, 1982, unpublished.
38. V.N. Kurlov, B.M. Epelbaum, *J. Crystal Growth*, v. 179, 1997, p. 175.
39. P.I. Antonov, Yu.G. Nosov, S.P. Nikanorov, *Bull. Acad. Sci. USSR, Phys. Ser.*, v. 49, 1985, p. 6.
40. C.P. Khattak, F. Schmid, *Mater. Lett.*, v. 7, No 9/10, 1989, p. 318.
41. A. Horowitz, S. Biderman, D. Gazit, Y. Einav, G. Ben-Amar and M. Weiss, *J. Crystal Growth*, v. 128, 1993, p. 824.
42. J.W. Locher, H.E. Bennet, P.C. Archibald and C.T. Newmyer, in: *Window and Dome Technologies and Materials II*, SPIE Proc., v. 1326, 1990, p. 2.
43. A.V. Nikiforov, Yu.G. Nosov, O.V. Kljavin, P.I. Antonov, M.B. Mikhamedzhanova, *Bull. Acad. Sci. USSR, Phys. Ser.*, v. 52, 1988, p. 131.
44. V.A. Borodin, V.V. Sidorov, S.N. Rossolenko, T.A. Steriopo, V.A. Tatarchenko, *J. Crystal Growth*, v. 104, 1990, p. 69.
45. V.N. Kurlov, F. Théodore, *Cryst. Res. Technol.*, v. 34, 1999, p. 293.
46. P.A. Gurjiyants, M.Yu. Starostin, V.N. Kurlov, F. Théodore, J. Delepine, *J. Crystal Growth*, v. 198/199, 1999, p. 227.
47. R.L. Gentilman in: *Infrared and Optical Transmitting Materials*, Ed. R.W. Schwartz, SPIE, v. 683, 1986, p. 2.

48. F. Théodore, T. Duffar, J.L. Santailier, J. Pesenti, M. Keller, P. Dusserre, F. Louchet, V.N. Kurlov, *Bull. Rus. Acad. Sci., Physics*, v. 63, 1999, p. 1686.
49. F. Théodore, T. Duffar, J.L. Santailier, J. Pesenti, M. Keller, P. Dusserre, F. Louchet, V.N. Kurlov, *J. Crystal Growth*, v. 198/199, 1999, p. 317.
50. V.M. Krymov, V.N. Kurlov, P.I. Antonov, F. Théodore, J. Delepine, *J. Crystal Growth*, v. 198/199, 1999, p. 210.
51. "Physics and Spectroscopy of Laser Crystals" (Ed. A.A. Kaminsky), Nauka, Moscow 1986, (in Russian).
52. V.N. Kurlov, S.V. Belenko, *Advanced Materials*, v. 10, 1998, p. 539.
53. V.N. Kurlov, S.V. Belenko, *Inorganic Materials*, v. 34, 1998, p. 571.
54. V.N. Kurlov, S.V. Belenko, *J. Crystal Growth*, v. 191/4, 1998, p. 779.
55. B.M. Epelbaum, K. Shimamura, V.V. Kochurikhin, T. Fukuda, *Cryst. Res. Technol.*, v. 33, 1998, p. 787.
56. C.A. Burrus, L.A. Coldren, *Appl. Phys. Lett.*, v. 31, 1977, p. 383.
57. P. Rudolph, K. Shimamura, T. Fukuda, *Cryst. Res. Technol.*, v. 29, 1994, p. 801.
58. L.N. Dmitruk, *Bull. Acad. Sci. USSR, Phys. Ser.*, v. 49, 1985, p. 130.
59. K. Shimamura, N. Kodama, T. Fukuda, *J. Crystal Growth*, v. 142, 1994, p. 400.
60. V.N. Kurlov, S.N. Rossolenko, S.V. Belenko, *J. Crystal Growth*, v. 191, 1998, p. 520.
61. V.N. Kurlov, S.N. Rossolenko, *J. Crystal Growth*, v. 173, 1997, p. 417.
62. V.N. Kurlov, S.V. Belenko, *Inorganic Materials*, v. 34, No 12, 1998, p. 1233.
63. E.R. Dobrovinskaya, L.A. Litvinov, V.V. Pishchik, *J. Crystal Growth*, v. 50, 1980, p. 341.
64. V.A. Tatarchenko, T.N. Yalovets, G.A. Satunkin, L.M. Zatulovsky, L.P. Egorov, D.Ya. Kravetsky, *J. Crystal Growth*, v. 50, 1980, p. 335.
65. R.E. Novak, R. Metzl, A. Dreeben, S. Berkman, D.L. Patterson, *J. Crystal Growth*, v. 50, 1980, p. 143.
66. K. Wada, K. Hoshikawa, *J. Crystal Growth*, v. 50, 1980, p. 151.
67. I. Nicoară, D. Nicoară, V. Sofonea, *J. Crystal Growth*, v. 104, 1990, p. 169.
68. V.A. Tatarchenko "Stable crystal growth", Moscow, Nauka, 1988, p. 135, (in Russian).
69. V.N. Kurlov, S.N. Rossolenko, *Bull. Rus. Acad. Sci., Physics*, v. 63, No 9, 1999, p. 1711.
70. V.N. Kurlov, B.M. Epelbaum, S.N. Rossolenko, *Bull. Rus. Acad. Sci., Physics*, v. 63, No 9, 1999, p. 1705.



Professor Peter I. Antonov graduated from the St. Petersburg State University in 1958. Then he joined the A.F. Ioffe Physical Technical Institute, Russian Academy of Sciences where he worked up to present. He was engaged in shaped crystal growth by the Stepanov method. Main directions of his activity are: regularity and controlling of shaped melt column, thermal stresses, origin of structural defects, development of a new versions of the Stepanov method. Hi is an organizer of Russian Conferences on shaped crystal growth.



Dr. Vladimir Kurlov was educated at the M.V. Lomonosov Moscow Institute of Fine Chemical Technology in 1982, where he obtained MSc in technology of special materials for electronics. Then he joined the Institute of Solid State Physics, Russian Academy of Sciences where he worked up to present. He was engaged in crystal growth from the melt. He received a Ph.D. degree in Solid State Physics in 1992 in the Institute of Solid State Physics. Dr Kurlov worked for 1.5 year (1995/1997) as a researcher at CEA/CEREM, Grenoble, France.

Dr V.N. Kurlov is the author of over 50 research papers and reviews concerning the crystal growth from the melt. He has 25 Russian and European Patents in crystal growth field.